ETEC heat-labile toxin promotes β-catenin stabilization and transcriptional reprogramming to disrupt intestinal epithelial differentiation

Alaullah Sheikh[1*], Bipul Setu[1], Nikhilesh Joardar[1†], John C. Martin[1], Bruce A. Rosa, [1] Makedonka Mitreva[1,2,3], James M. Fleckenstein[1,4*]

[1]Division of Infectious Diseases, Department of Medicine, Washington University in Saint Louis School of Medicine, Saint Louis, Missouri, USA; [2]Department of Genetics, Washington University in Saint Louis School of Medicine, Saint Louis, Missouri, USA; [3]McDonnell Genome Institute, Washington University in Saint Louis School of Medicine, Saint Louis, Missouri, USA; [4]Medicine Service, Infectious Disease Section, Veterans Affairs Health Care System, Saint Louis, Missouri, USA.

†Present address- Department of Bioengineering, School of Engineering and Technology, Dr. Vishwanath Karad MIT World Peace University, Maharashtra, India.

***Co-corresponding authors**

Alaullah Sheikh
Division of Infectious Diseases
Department of Medicine
Washington University School of Medicine
Campus Box 8051
660 South Euclid Avenue
Saint Louis Missouri, USA 63110
p 314-362-9219
asheikh@wustl.edu

James M. Fleckenstein
Division of Infectious Diseases
Department of Medicine
Washington University School of Medicine
Campus Box 8051
660 South Euclid Avenue
Saint Louis Missouri, USA 63110
p 314-362-9218
jfleckenstein@wustl.edu

Abstract

Enterotoxigenic *Escherichia coli* (ETEC), defined by their production of heat-labile (LT) and heat-stable (ST) enterotoxins, are a common cause of acute diarrheal illness in children from low- and middle-income countries, and are also linked to long-term sequelae such as malnutrition, and growth impairment. While the mechanisms underlying toxin-mediated acute diarrhea are known, the molecular events involved in ETEC related sequelae remain unclear. Here, we demonstrate that the ETEC heat-labile toxin (LT) profoundly remodels intestinal epithelial composition and function through modulation of WNT/β-catenin signaling. Using human ileal enteroids, we demonstrate that LT stabilizes β-catenin independently of WNT ligands, promotes its nuclear accumulation, and enhances TCF/LEF-driven transcription. Single-cell transcriptomic analyses reveal that LT increases intestinal proliferation by enhancing cell cycle activity across all epithelial lineages, thus disrupting epithelial composition by expanding proliferative progenitor populations at the expense of absorptive enterocytes. Simultaneously, LT impairs epithelial maturation and suppresses transcriptional programs required for nutrient absorption and differentiation. Together, these findings identify LT as a potent driver of intestinal epithelial reprogramming, providing mechanistic insight into how ETEC infection may drive long-term consequences beyond acute diarrhea and may inform strategies to prevent major sequelae, including malnutrition, that affect millions of children worldwide.

51 ## Introduction

52 The enterotoxigenic *E. coli* (ETEC) are a diverse group of diarrheal pathogens defined by their
53 production of heat-labile (LT) and/or heat-stable (ST) enterotoxins[1]. The ETEC pathovar is thought to be
54 responsible for hundreds of millions of cases of diarrheal illness each year, primarily among young
55 children of low-middle income countries (LMICs)[2]. Children of LMICs frequently suffer multiple episodes
56 of ETEC diarrhea before in the first few years of life[3], and ETEC are a leading cause of death due to
57 diarrheal illness in children under the age of five years[4]. While the death rate from acute diarrheal
58 illness has declined with advances in oral rehydration therapy and other measures, children with ETEC
59 diarrhea are also at increased risk of death after resolution of the initial episode[5]. Moreover, children
60 with moderate-severe diarrhea[6] as well as less severe diarrhea[7] due to ETEC inexplicably suffer long-term
61 sequelae including from a condition referred to as environmental enteric dysfunction (EED) characterized
62 histologically by atrophy of small intestinal villi accompanied by expansion of crypts[8,9], and clinically by
63 poor growth and malnutrition. Unfortunately, in the absence of a licensed vaccine, morbidity due to
64 acute diarrheal illness as well as long-term sequelae of impaired growth and malnutrition have
65 continued unabated[7].

66 The fundamental molecular pathogenesis of acute diarrheal illness caused by ETEC is well-
67 established. Delivery of LT and ST activates production of cAMP and cGMP cyclic nucleotides,
68 respectively. Increases in intracellular cAMP leads to activation of protein kinase A (PKA) while cGMP
69 activates protein kinase G (PKG). Kinase-mediated phosphorylation of cellular ion channels in enterocyte
70 membranes leads to the net export of salt and water into the intestinal lumen, culminating in profuse
71 watery diarrhea characteristic of ETEC.

72 In contrast, the sequelae linked to ETEC are still poorly understood. Recently, however we
73 demonstrated that heat-labile toxin modulates the transcription of hundreds of genes in target intestinal
74 epithelial cells, including those responsible for the biogenesis of enterocyte microvilli responsible

75 nutrient absorption[10]. Moreover, repeated challenge of infant mice with toxigenic ETEC leads to impaired
76 growth[10] similar to observations in children. These studies provided the first suggestion that ETEC toxins
77 might drive molecular events that culminate in sequelae.

78 Nutrient absorption in the small intestine depends on tightly regulated epithelial differentiation and
79 maturation processes that generate functionally specialized cell types. Intestinal stem cells (ISCs),
80 residing at the base of crypts, undergo proliferation and lineage specification to give rise to absorptive
81 enterocytes and secretory lineages including goblet, Paneth, and enteroendocrine cells[11]. As these cells
82 migrate along the crypt-villus axis, they progressively differentiate, acquiring mature phenotypes and
83 functional attributes[12]. In particular, enterocytes undergo a stepwise transcriptional and morphological
84 maturation program culminating in the expression of solute carrier (SLC) transporters, and other
85 molecules essential for nutrient uptake and barrier function[13]. Theoretically, disruption of this
86 developmental trajectory would compromise nutrient absorption and contribute to malnutrition among
87 children from low-resource settings[8,14-17].

88 Intestinal epithelial maturation is tightly regulated. The luminal surface of the small intestine is
89 comprised of millions of villi, tiny (~0.5 mm long) fingerlike projections that are surrounded at their base
90 by invaginations known as crypts. As epithelial cells covering the villi are propagated from intestinal stem
91 cells (ISC) residing in the crypts they quickly differentiate into mature epithelial cells, with absorptive
92 enterocytes covered in microvilli making up the majority. These mature cells on the villous surface
93 undergo continual renewal over a period of 3-5 days[18] as they are constantly replenished by the
94 population of crypt stem cells. Differentiation of ISC into enterocytes and other cell types along the
95 crypt-villus axis is controlled by a number of signaling molecules including WNT[19-21].

96 High concentrations of WNT generated by adjacent Paneth cells[22] favor the maintenance and
97 proliferation of crypt (ISC) populations. In the absence of WNT, a "destruction complex" comprised of
98 GSK-3 β, CK1α, APC, and Axin2 engages β-catenin. GSK-3 β phosphorylation of β-catenin targets it for

99 ubiquitination[23] and removal from the cytoplasm. Binding of WNT to its cognate LRP5/6-Frizzled co-
100 receptors on the cell surface activates Dishevelled, a cytoplasmic protein that antagonizes the
101 destruction complex[24]. This permits accumulation of monomeric β-catenin in the cytoplasm[25] and
102 ultimately its translocation to the nucleus where it binds to T-cell factor (TCF) and lymphoid enhancer
103 factor (LEF) transcription factors[26], leading to activation of WNT/TCF target genes responsible for
104 maintenance of the crypt progenitor cells. In addition to canonical WNT signaling, β-catenin can be
105 stabilized both directly and indirectly by modulating features of the destruction complex. Here, we
106 demonstrate that heat-labile enterotoxin of ETEC enhances β-catenin stabilization to activate
107 downstream signaling in small intestinal epithelia, disrupting differentiation and maturation required for
108 efficient nutrient uptake.
109

110 ## Results

111 ### Heat-labile toxin activates transcription of multiple WNT-responsive genes

112 Bioinformatic analysis (CompBio v2.9) of earlier bulk RNAseq data[10] from small intestinal enteroids
113 treated heat-labile toxin revealed that transcription of genes governed by the WNT-β-catenin pathway
114 were significantly upregulated in response to LT (figure 1a). Upregulated genes included Axin2, RNF43,
115 MYC, SOX9, cyclin D1 (CCND1), EphB2, LGR5, PROM1, DKK1, CLDN1, TSPAN8, along with a number of
116 other genes governing the intestinal cell differentiation including OLFM4, CD24, REG4, XBP1, and
117 ATOH1[21,27,28]. Using CEACAM6 as a positive control[29] for LT-induced gene expression, we validated impact
118 on genes in this pathway by qRT-PCR (Figure 1b). In keeping with these results, we also observed cellular
119 accumulation of β-catenin following treatment of polarized small intestinal enteroids with LT (Figure
120 1c,d).

121 To functionally assess transcriptional modulation by β-catenin, we stably transfected small intestinal
122 enteroids with a lentivirus vector construct (7TFP)[30] which contains 7 copies of the TCF/LEF transcription

123 factor DNA-binding site 5'-CCTTTGATC-3' upstream of firefly luciferase[31]. Treatment of 7TFP carrying
124 reporter enteroids with LT resulted in significant increases in TCF/LEF-mediated transcriptional activity
125 (Figure 1e). These effects were abrogated when the enzymatically inactive mutant form of LT (mLT) was
126 used, indicating that catalytic activity of LT is required for this activation.

127 **Heat-labile toxin stabilizes cytosolic β-catenin to facilitate nuclear translocation**

128 In canonical WNT signaling pathways, β-catenin accumulation in the nucleus permits engagement of
129 TCF/LEF transcription factors to activate transcription of downstream genes (Figure 2a). Interestingly,
130 activation of cyclic nucleotide pathways has the potential to interfere with degradation of β-catenin. PKA
131 phosphorylation of β-catenin at position Ser_{675} inhibits β-catenin ubiquitination, thereby permitting its
132 accumulation[32], while activation of PKA can also result in phosphorylation of GSK-3β at Ser_9 resulting in
133 its inhibition[33-37]. Similarly, cGMP activation of PKG also results in phosphorylation of GSK-3β at Ser_9[38,39]
134 to inhibit enzymatic activity. Accordingly, we observed time-dependent increases in total β-catenin in
135 both cytoplasmic and nuclear compartments (Figure 2b-e). In parallel, LT induced phosphorylation of β-
136 catenin at Ser_{675} (Figure 2b-e, Supplementary figure 1), a known activating modification that promotes β-
137 catenin nuclear localization and transcriptional activity[40], further supporting functional stabilization.

138 In addition, we found that LT modulated phosphorylation of GSK-3β, a central negative regulator of β-
139 catenin stability. Although total protein levels remained relatively unchanged, GSK-3β phosphorylation at
140 the Ser_9 residue increased significantly in LT-treated samples over time (Figure 2b, d).

141 Collectively, these data demonstrate that heat-labile toxin acts to stabilize β-catenin independent of
142 WNT by directed post translational modification of β-catenin and elements of the destruction
143 complex[32,41]. Interestingly, we also noted that transcription of the *CTNNB1* gene encoding β-catenin was
144 itself upregulated in response to LT, potentially related to the presence of cAMP response elements[42] in
145 the CTNNB1 promoter[43].

146 **Heat-labile toxin disrupts epithelial cell composition**

147 Given the central role of WNT/β-catenin signaling in regulating intestinal stem cells[20] and their
148 differentiation to different epithelial cell types[18], we next investigated whether LT-induced stabilization of
149 β-catenin impacts epithelial cell dynamics. In the intestine, proliferative expansion without coordinated
150 differentiation can shift the cellular composition and impair epithelial function[44]. To investigate whether
151 heat-labile toxin perturbs this balance, we used single-cell RNA sequencing to examine the impact of LT
152 on differentiation of human small intestinal enteroids. Control (Ø) and LT-treated enteroid cells were
153 harvested and subjected to Illumina NovaSeq X Plus single-cell RNA sequencing, followed by analysis
154 with Seurat (v5.0)[45]. After quality control filtering, 1,963 cells represented by an average of 14,342 reads
155 and 3,266 genes were sequenced in the control sample, and 2207 cells, an average of 14,099 reads and
156 3283 genes in the LT sample. To assess changes in epithelial cell composition, we then performed
157 unsupervised graph-based clustering of single-cell transcriptomes from control and LT-treated enteroids
158 (resolution setting of 0.92, defining 14 clusters), followed by annotation using canonical lineage
159 markers[11,13], confidently identifying all expected major cell types (Figure 3a; Table 1; **Supplementary**
160 **dataset 1**).

161 LT treatment induced striking alterations in enteroid cell composition. All major intestinal epithelial
162 cell types, including absorptive enterocytes, goblet cells, Paneth cells, and enteroendocrine cells, along
163 with intermediate populations likely representing transitional states along the differentiation axis, were
164 identified in both control and LT-treated samples (Figure 3a–c). However, a highly proliferative cluster,
165 largely absent in controls, was markedly expanded following LT exposure, while a differentiated
166 population present only in control samples was lost (Figure 3d–e). Differential abundance analysis
167 confirmed enrichment of early-stage progenitor and transit-amplifying populations (Clusters 0, 7, and 8)
168 in LT-treated samples, alongside significant depletion of mature enterocytes (Clusters 4 and 5) and
169 BEST4^{+} absorptive cells (Cluster 13) (Figure 3e; Table 1).

170 To further explore the identity of these transcriptionally distinct or depleted populations (Clusters 7,
171 and 13, respectively) in LT-treated enteroids, we performed over-representation analysis (ORA). ORA of
172 cluster 7 revealed strong enrichment for mitotic cell cycle pathways, including G2/M transition, spindle
173 checkpoint, and DNA replication, indicating a highly proliferative state (Supplementary figure 2a).
174 Consistently, transcription factor analysis identified dominant enrichment of E2F family regulators (E2F1,
175 E2F2, E2F3) and their partners DP1/DP2, which are key drivers of S-phase entry and DNA synthesis
176 (Supplementary figure 2b). Additional enriched motifs included MYC, NFY, and YY1, supporting enhanced
177 biosynthetic and metabolic activity consistent with transit-amplifying cells. In contrast, Cluster 13 was
178 enriched for pathways associated with terminal epithelial differentiation and absorptive function. These
179 included mitochondrial respiration, oxidative phosphorylation, the TCA cycle, and lipid metabolism
180 (Supplementary figure 2a). The absence of proliferative transcription factor signatures in Cluster 13
181 further supports its identity as a mature enterocyte population (Supplementary figure 2b). Together,
182 these findings reveal that LT exposure promotes the expansion of transcriptionally active proliferating
183 cells while depleting functionally mature absorptive cells, disrupting the balance between proliferation
184 and differentiation in the intestinal epithelium.
185 To gain deeper insight into the transcriptional alterations underlying these shifts, we conducted
186 differential gene expression analysis on all cell clusters, identifying thousands of differentially expressed
187 genes (DEGs) significantly upregulated or downregulated in LT-treated enteroids compared to control
188 (Table 2, **Supplementary dataset 2**). To assess functional implications, we performed over-representation
189 analysis (ORA) of differentially expressed genes. Upregulated DEGs were enriched for pathways in RNA
190 metabolism, cell cycle regulation, and stress response, consistent with a proliferative epithelial state
191 (Supplementary figure 3). Downregulated DEGs were enriched for bile acid transport, lipid metabolism,
192 cholesterol biosynthesis, and other absorptive functions, indicating impaired maturation and loss of
193 differentiation (Supplementary figure 3). Gene ontology independent analysis (CompBio v2.9) likewise

194 highlighted suppression of metabolic and transport functions, including intestinal absorption, lipid and
195 bile metabolism, fatty acid uptake, amino acid metabolism, and cholesterol processing (Supplementary
196 figure 4, also see **Supplementary dataset 2**). Taken together, these data indicate that LT exposure drives
197 a shift in epithelial composition by promoting proliferation and suppressing differentiation.

198 **Heat-labile toxin promotes intestinal epithelial cell proliferation and reshapes cell cycle dynamics**
199 **across epithelial cell clusters**

200 Because proliferation kinetics directly influence epithelial cell-type composition[44], we next examined
201 how LT affects the cell cycle status of intestinal epithelial cells. Using canonical gene sets for G1, S, and
202 G2/M phases[46] (Supplementary figure 5a), we assigned cell cycle stages to individual cells in LT-treated
203 and control enteroids. UMAP projections revealed a marked shift in overall cell cycle distribution upon LT
204 exposure (Figure 4a). Specifically, LT-treated cells showed a significant expansion of S-phase ($p = 2.21 \times$
205 10^{-5}, χ^2) and G2/M-phase populations ($p < 1 \times 10^{-16}$), accompanied by a reduction in G1-phase cells (Table
206 3).

207 Cell cycle phase scores further confirmed these shifts, with elevated expression of S-phase and G2/M
208 gene sets in LT-treated enteroids (Figure 4b). Consistent with this, we observed differential expression of
209 key phase-specific cell cycle regulators, including RB1 and CDKN1A (G1-phase), PCNA and MCM3 (S-
210 phase), and CCNB2 and CDK1 (G2/M-phase) (Figure 4c). LT exposure also upregulated stem and
211 progenitor markers such as CD24, CD44, and OLFM4, reinforcing the expansion of the undifferentiated,
212 proliferative compartment (Supplementary figure 5b).

213 Compartmentalization of intestinal cell proliferation is critical for epithelial maintenance and function
214 with higher proliferative activity at the crypt zone and no proliferation at the tips of villi. Analysis of cell
215 cycle dynamics across transcriptionally defined clusters revealed a widespread reduction in G1-phase
216 cells and robust enrichment of G2/M-phase cells across epithelial subpopulations (Figure 5a; Table 3),
217 indicating that LT alters cell cycle dynamics across the entire epithelial landscape.

218 To further support the observed shift in cell cycle dynamics, we analyzed the expression of canonical
219 proliferation markers. LT-treated enteroids exhibited strong upregulation of MKI67 and TOP2A, two well-
220 established indicators of active proliferation[47] (Figure 5b). To validate these transcriptomic findings at the
221 protein level, we performed phenotypic assays using polarized epithelial monolayers. Enteroids were
222 cultured on Transwell filters to establish apical–basolateral polarity and treated with LT during the
223 differentiation phase. Confocal immunofluorescence microscopy revealed a significant increase in
224 $MKI67^{+}$ nuclei in LT-treated monolayers compared to controls (Figure 5c-d), confirming enhanced
225 proliferative activity at the protein level.
226 To functionally validate these observations, we utilized 5-ethynyl-2'-deoxyuridine (EdU) incorporation
227 assay in 3D culture of enteroids treated with LT. Following differentiation, both control and LT-treated
228 enteroids were incubated with EdU. LT treatment led to significantly higher incorporation of EdU
229 ($p<0.01$), indicating enhanced DNA synthesis and entry into S phase (Figure 5e–f). Collectively, these
230 findings indicate that LT skews epithelial homeostasis by promoting a proliferative, progenitor-dominated
231 state across the intestinal epithelium.
232

233 **Heat-labile toxin suppresses epithelial differentiation and impairs functional maturation**

234 Given this marked shift away from differentiated lineages, we next investigated whether LT-induced
235 disruption of differentiation affects epithelial maturation. Villin, a structural component of apical
236 microvilli, and intestinal alkaline phosphatase (ALPI), a brush-border enzyme, serve as canonical markers
237 of mature enterocytes[12,48]. To assess the functional consequences of LT-induced differentiation defects,
238 we examined villin and ALPI protein expression in membrane and cytosolic fractions, respectively, from
239 control and LT-treated enteroids. Consistent with the transcriptional changes (Supplementary Figure 6a),
240 immunoblot analysis showed significantly reduced expression of villin, and alkaline phosphatase (ALPI),

241 in LT-treated enteroids compared to controls (Figure 6a–b), suggesting impaired epithelial maturation at
242 the protein level.

243 To further investigate the impact of LT on the functional maturation of the epithelia, we examined the
244 expression of key solute carrier (SLC) genes responsible for nutrient transport. Although we observed
245 robust expression of multiple SLC family members in control enteroids, LT-treated enteroids exhibited
246 marked repression of these genes across the epithelial cell clusters (Supplementary figure 6b). Notably,
247 LT diminished the expression of SLC28A1 (nucleoside), SLC23A1 (vitamin C), SLC30A1/30A4 (zinc),
248 SLC7A7 (amino acids), SLC5A11 (myo-inositol), SLC19A3 (thiamine), SLC11A2 (iron), SLC17A4
249 (glutamate), SLC15A1 (di/tripeptides), and other transporters (Supplementary figure 7), consistent with a
250 depletion of functionally mature enterocytes.

251 Because nutrient absorption is a key functional hallmark of mature enterocytes, we next analyzed the
252 transcriptional consequences of LT treatment on nutrient transporter expression across five
253 transcriptionally defined enterocyte subclusters (EC1–EC5). LT exposure led to a global reduction in
254 transporter gene expression scores across multiple categories, including sugar, amino acid, water, bile
255 acid, lipid, and vitamin transport (Figure 6c, left). This was further supported by reduced average
256 expressions and cell-level prevalence of multiple solute carrier (SLC) family genes[12] in LT-treated cells
257 compared to controls (Figure 6c, right).

258 Consistent with these observations, prior bulk RNA-seq studies have shown that LT suppresses
259 SLC19A3, a thiamine transporter, along with its upstream regulator SP1, leading to impaired thiamine
260 uptake[49]. Our single-cell RNA-seq data recapitulated this finding, with decreased expression of both
261 SLC19A3 and SP1 in LT-treated enteroids (Figure 6d). Additionally, differential gene expression analysis of
262 enterocyte clusters revealed significant downregulation of other key absorptive genes, including SLC5A1
263 (sodium/glucose cotransporter 1), SLC10A2 (ileal sodium/bile acid cotransporter), SLC28A1

264 (sodium/nucleoside cotransporter 1), FABP6 (fatty acid transporter), and APOB (fatty acid transporter),

265 confirming suppression of essential nutrient acquisition pathways (Figure 6e).

266 Altogether, these studies suggest that LT exerts a profound effect on the developing intestinal

267 epithelia. The LT-driven proliferative response coincided with transcriptional activation of WNT/β-catenin

268 target genes and nuclear accumulation of β-catenin, consistent with canonical WNT pathway activation.

269 By impacting major transcriptional pathways, including those orchestrated by β-catenin, LT disrupts

270 epithelial differentiation and subsequent maturation.

271 ## Discussion

272 ETEC infections have repeatedly been linked to long-term sequelae including malnutrition and
273 impaired growth, significantly compounding the morbidity burden beyond the acute infection [5,8,15,16,50,51].
274 While LT-producing ETEC have specifically been linked to malnutrition among young children[50], the
275 precise molecular mechanisms underlying links between ETEC and nutritional sequelae remain
276 incompletely understood. The present studies suggest that LT may alter the trajectory of epithelial cell
277 maturation, stalling the development of mature absorptive enterocytes. This disruption of normal
278 epithelial homeostasis parallels earlier observations that LT also interferes with transcriptional programs
279 that govern the biogenesis of enterocyte microvilli, comprising the major surface for nutrient absorption,
280 along with LT modulation of a multitude of nutrient transporters[52]. The collective impacts of LT on the
281 architecture and function of absorptive intestinal epithelia likely contribute significantly to the
282 nutritional deficits that accompany ETEC infections in young children.

283 Here we show that the heat-labile enterotoxin reprograms intestinal epithelia by subversion of the
284 fundamental regulation of stem cell maintenance, proliferation, and differentiation[18,53,54] governed by β-
285 catenin. While LT is classically known for inducing diarrhea via cAMP-mediated chloride secretion[55,56], its
286 broader impact on intestinal development has remained poorly characterized. Here, we show that LT
287 activates β-catenin signaling independent of WNT by stabilizing β-catenin through PKA-mediated
288 phosphorylation of β-catenin and components of its degradation complex[32,57,58]. The resulting enhanced
289 and aberrant β-catenin signaling ultimately reprograms homeostatic maturation of intestinal epithelia.

290 The intricate nature of cAMP and PKA signaling is reflected in complex array of changes that follow
291 exposure to heat-heat labile toxin. Mechanistically, LT modulates transcriptional programs by PKA-
292 mediated phosphorylation of a family of cAMP-responsive nuclear factors including the cAMP response
293 element binding protein (CREB) and the cAMP response element modulator (CREM), permitting their
294 interaction with transcriptional co-activators including CREB-binding protein (CBP) as they bind

295 cooperatively to short DNA consensus sequences known as cAMP response elements (CRE)[59] in the
296 promoter regions of target genes. Intriguingly, genetic studies in Bangladeshi children identified CREM
297 polymorphisms associated with increased susceptibility to diarrhea and reduced weight-for-age[60],
298 potentially supporting the involvement of cAMP signaling in nutritional sequelae.

299 The cAMP pathway is also at the center of complex regulatory cascades involving multiple
300 transcription factors in addition to CREB and CREM that are also modulated by PKA[59]. These include the
301 transcriptional regulators HNF4A and SMAD4, both essential for enterocyte differentiation and known to
302 be sensitive to PKA-dependent phosphorylation[61,62 63-65]. Beyond direct transcriptional effects, cAMP-
303 driven activation of co-regulators such as CBP and PHF2 can induce histone acetylation and methylation,
304 also raising the possibility that LT reinforces impaired epithelial maturation through epigenetic
305 remodeling[62].

306 Our data supports the view that LT activates β-catenin signaling to impair terminal enterocyte
307 differentiation. Under homeostatic conditions, β-catenin regulates the balance between stem cell
308 renewal and lineage commitment in the crypt-villus axis[21,86-88]. Disruption of this axis, such as through
309 loss of WNT antagonists like APC, leads to crypt expansion and impaired epithelial maturation [21,66,67]. Our
310 findings align with this paradigm, showing that LT mimics hyperactive WNT signaling to expand
311 progenitor and transit-amplifying populations while depleting differentiated lineages, including mature
312 enterocytes and BEST4^{+} absorptive cells[68]. This imbalance is characteristic of a poorly differentiated
313 epithelium and closely mirrors the pathological features of environmental enteric dysfunction (EED),
314 characterized by villus blunting, crypt expansion, and malabsorption[69,70].

315 The depletion of mature absorptive cells and downregulation of nutrient transporter genes in LT-
316 treated enteroids recapitulate key features of immature epithelia. Epithelial maturation involves
317 functional enrichment of nutrient absorption capacity in villus tip cells, where genes required for brush

318 border formation and fat absorption are upregulated in differentiated villus enterocytes[12]. However, LT-
319 treated epithelia exhibit reduced expression of ALPI, and VIL1, canonical markers of enterocyte
320 maturation, as well as transcriptional repression of multiple solute carrier family genes essential for
321 absorptive functions of nutrient, bile acid, and vitamin transport. The failure to achieve mature
322 enterocyte identity is particularly relevant in the context of EED, where altered bile acid metabolism and
323 nutrient malabsorption are linked to stunted growth. Notably, a study in undernourished Pakistani
324 infants found that disrupted bile acid homeostasis correlated with EED histopathology and growth
325 faltering[71]. LT-induced repression of bile acid transporters (SLC10A2, FABP6) may offer a plausible
326 mechanistic link to these clinical observations.

327 This concept is further supported by recent animal studies, where bile acid accumulation and NAD^+
328 deficiency induced by a low-protein diet led to villus atrophy and epithelial loss, phenotypes that were
329 reversed by dual supplementation with NAD^+ precursors and bile acid sequestrants [72]. Our findings raise
330 the possibility that LT could act synergistically with nutritional stressors to maintain an immature
331 epithelial state, exacerbating malabsorption and stunting in vulnerable children. The ability of LT to
332 disrupt intestinal maturation and impair nutrient uptake underscores the pathogenic potential of ETEC
333 beyond acute diarrhea.

334 From a broader perspective, this work positions LT as a potential molecular link between ETEC
335 infection and long-term intestinal dysfunction. The sustained shift toward a proliferative,
336 undifferentiated epithelial state, driven by toxin-mediated signaling, mirrors intestinal phenotypes
337 observed in chronically infected or malnourished children, where impaired differentiation contributes to
338 long-term functional deficits[8,16,17,73]. These findings are especially concerning in the context of repeated
339 or chronic ETEC exposure, which is common in low-resource settings and has been linked to growth
340 faltering in children even in the absence of overt diarrhea[15,50,51,74-78].

341 While this study provides mechanistic insight into LT-induced epithelial reprogramming, several
342 limitations should be noted. First, the findings are based on *in vitro* enteroid models, which lack stromal,
343 immune, and microbial components that shape epithelial responses *in vivo.* Second, although we
344 identify β-catenin signaling as a key mediator, the specific upstream effectors connecting LT-induced
345 cAMP production to transcriptional reprogramming remain to be fully defined. In addition to LT, many
346 ETEC make heat-stable toxins (ST) which engage guanylate cyclase C (GC-C) to stimulate production of
347 cGMP and activation of protein kinase G (PKG). Although ST has not been thoroughly evaluated in the
348 context of EED, ST and other GC-C agonists are known to impact cell cycle progression and modulate
349 epithelial proliferation and differentiation[79-81].

350 Understanding how these common enterotoxins contribute to pathogenesis of intestinal dysfunction
351 that follow ETEC infections can inform the rational design of vaccines that protect against acute illness as
352 well as the tremendous burden of sequelae[52,82]. This work advances our understanding of how ETEC
353 contributes to long-term intestinal dysfunction and malnutrition and offers a framework for developing
354 strategies to mitigate the persistent sequelae of enteric infections in vulnerable populations.

355

356 ## Materials and methods

357 All experiments were conducted in accordance with relevant ethical guidelines, and study protocols
358 were approved by the Institutional Biosafety Committee (IBC), and Institutional Review Board (IRB) at
359 Washington University School of Medicine in St. Louis.

360 ### Growth and maintenance of small intestinal enteroid cell lines

361 Hu235D derived from human small intestinal (ileal) stem cells were obtained from the Precision
362 Animal Models and Organoids Core (PAMOC) maintained by the Washington University Digestive
363 Diseases Research Core Center (DDRCC), and were propagated as previously described[83]. Briefly, crypt
364 intestinal stem cells maintained in liquid nitrogen were thawed, resuspended in Cultrex (Cultrex BME
365 Type II, Catalog# 3532-010-02, Biotechne) and transferred to wells in a 48-well plate. Cells were grown
366 for 3-4 days in growth media containing 50% L-WRN conditioned media derived from the L-WRN cell line
367 (provided by the POMAC), a 1:1 mixture of primary media [Advanced DMEM/F12, Invitrogen 12634028,
368 supplemented with fetal bovine serum (FBS, 20%), 2 mM L-glutamine, 100 U/ml penicillin, 0.1 mg/ml
369 streptomycin], 10 µM ROCK inhibitor Y-27632 (Tocris Bioscience) and 10 µM TGFBR1 inhibitor SB 431542
370 (Tocris Bioscience) [83] [84].

371 For RNA-seq analysis, cells were grown in Cultex for 4 days for enteroid formation, diluted 1:2 in
372 Cultrex to reduce enteroid density, replated and grew for 3 more days in growth media. To allow
373 differentiation, enteroids were then cultured for additional 3 days in differentiation media (5% L-WRN
374 conditioned media supplemented with 10 µM ROCK inhibitor). Enteroids were treated with heat-labile
375 toxin (100ng/ml) either during the differentiation period (LT), or PBS treated (control).
376 For polarized enteroid monolayers, following trypsinization cells were seeded onto Transwell filters
377 (Corning) coated with type IV human collagen (Sigma) and grew in growth media for confluent
378 monolayer. After confluency growth, media was replaced with differentiation media to promote
379 differentiation.

380 **Quantitative RT-PCR**

381 Quantitative real-time PCR was conducted on a QuantStudio 3 detection system (Applied Biosystems)
382 using Fast SYBR Green master mix (Applied Biosystems/Thermo Fisher). Specificity of amplification for
383 each sample was confirmed by dissociation curve analysis, and PCR product size was verified through
384 agarose gel electrophoresis. For transcript amplification from small intestinal enteroids, previously
385 described methods were followed, with relative gene expression normalized to GAPDH. All primers used
386 are provided in Supplementary table 1.

387

388 **Fluorescence microscopy**

389 For fluorescence microscopy, polarized enteroid monolayers were fixed in 2% paraformaldehyde for
390 30 minutes at 37°C, followed by an additional 30 minutes at room temperature. After fixation, the
391 monolayers were washed three times with PBS and blocked with 2% BSA-PBS to minimize non-specific
392 binding. The primary antibodies (as detailed in Supplementary table 2) used for labeling specific proteins
393 were diluted in 2% BSA-PBS and incubated with the monolayers for 1 hour at room temperature.
394 Fluorescent dye-conjugated secondary antibodies were then diluted in 2% BSA-PBS and applied to the
395 monolayers for 45 minutes at room temperature. Cell membranes and nuclei were stained using
396 CellMask (1:2000 dilution, Invitrogen) and DAPI (1:1000 dilution, Invitrogen), respectively. Slides were
397 washed 3x with PBS and coverslipped with Prolong Gold antifade reagent (Invitrogen). Images were
398 captured and analyzed using a Nikon C2 confocal microscope equipped with NIS-Elements AR 5.11.01
399 software (Nikon).

400 **Construction of TCF/LEF reporter enteroid lines.**

401 HEK293T cells (ATCC CRL-3216) were propagated at 37°C with 5% CO_2 in Dulbecco's Modified Eagle's
402 Medium (DMEM) supplemented with 10% heat-inactivated fetal bovine serum (FBS) and 2 mM L-
403 glutamine in T25 flasks. For 7TFP containing lentivirus production, cells were co-transfected with 5 µg of

404 p7TFP, 5 µg of psPAX2, and 3 µg of pMD2.G plasmids (see Supplementary table 3) in a 500 µl of culture
405 medium with 39 µl of FuGENE HD transfection reagent (Promega). Media was changed following 18 h
406 post transfection. Two days post transfection, the 7TFP-lentivirus–containing supernatant was collected,
407 clarified by centrifugation at 3,000 rpm for 15 minutes, and concentrated by adding polyethylene glycol
408 (PEG) 8000 at a 1:3 ratio (PEG:supernatant). The mixture was rotated overnight at 4°C and centrifuged at
409 1,600 × g for 1 hour. The resulting viral pellet was resuspended in 50% conditioned medium and used to
410 transduce Hu235D human small intestinal enteroids, in the presence of polybrene (final concentration:
411 8 µg/ml). After 8 hours at 37°C, cells were pelleted, resuspended in fresh Cultrex, and cultured for 3
412 days. Transduced cells were selected using puromycin (2.5 µg/ml) for p7TFP-expressing enteroids
413 (Hu235D::7TFP) and sorted in liquid nitrogen.

414 **7TCF/LEF Luciferase assays**

415 The Hu235D::7TFP cell line was resuspended in 50% L-WRN conditioned media enumerated
416 (Countess FL, ThermoFisher Scientific), and 35,000 live cells added in a total volume of 100 µl per well of
417 a 96 well plate (TPP, flat bottom, Cat# 92096) pre-coated with 3% Cultrex. After 48 hours growth at 5%
418 CO_2, 37°C, media was replaced with 5% L-WRN + Y-27632 to encourage differentiation. After 2 days, cells
419 in respective wells (~95% confluency) were treated with toxins as indicated in primary media only. After
420 equilibration to room temperature, 5'-fluoroluciferin reagent (ONE-Glo EX, E8110 Promega) was added
421 to wells and plates shaken at 200 rpm for 10 minutes. 120 µl from each well was then transferred to
422 corresponding wells of an opaque white 96 well plate (Microlite 1+, ThermoFisher 7417) and
423 luminescence measured (Synergy H1, BioTek). All treatments were performed at least in triplicate,
424 repeated at least three times.
425

426 ### Subcellular fractionation and immunoblotting

427 To isolate nuclear and cytoplasmic fractions, subcellular fractionation of human ileal enteroids was
428 performed using the NE-PER™ Nuclear and Cytoplasmic Extraction Kit (Thermo Fisher Scientific, #78833),
429 following the manufacturer's protocol with minor adaptations. Enteroids (~1×10^6 cells per condition)
430 were collected after treatment (e.g., with heat-labile toxin or PBS control), washed twice in ice-cold PBS,
431 and pelleted by centrifugation at 500 × g for 5 min at 4°C. Cytoplasmic and nuclear extracts were
432 sequentially isolated using the provided CER I, CER II, and NER buffers supplemented with Halt™
433 protease and phosphatase inhibitor cocktail (Thermo Fisher Scientific, #78440). After incubation with
434 CER I and CER II to lyse the cytoplasmic membrane, lysates were centrifuged at 16,000 × g for 5 min to
435 separate the supernatant for cytoplasmic fraction. The pellet was then resuspended in NER buffer and
436 incubated with vigorous vortexing every 10 min over a 40-min period. The nuclear fraction was collected
437 by centrifugation at 16,000 × g for 10 min. Protein concentrations were measured using a BCA assay
438 (Thermo Fisher Scientific), and fraction purity was confirmed by immunoblotting for cytoplasmic
439 (GAPDH) and nuclear (Lamin b1) markers. For immunoblotting, 10–30 µg of protein per sample was
440 mixed with Laemmli sample buffer containing 100 mM DTT, boiled at 95°C for 10 min, and resolved on
441 4–12% SDS-PAGE gels. Proteins were transferred to nitrocellulose membranes (100 V, 1 h) and blocked in
442 5% non-fat milk in PBS-Tween (0.1%). Membranes were incubated overnight at 4°C with primary
443 antibodies at 1:1000 dilutions (Supplementary table 2). After washing three times with PBST, HRP-
444 conjugated secondary antibodies (1:5,000) were applied for 1 h at room temperature. Signals were
445 developed using Clarity ECL substrate (BioRAD) and visualized with a c600 imager (azure Biosystems).
446 Band intensities were quantified using ImageJ and normalized to total protein across biological
447 replicates.

448 ### Single nuclei isolation for RNA sequencing

449 Following treatment, enteroids were collected in ice-cold PBS supplemented with 0.5 mM EDTA,
450 resuspended, and centrifuged at 200g for 5 minutes. For single-cell preparation, the cell pellets were
451 resuspended in TrypLE (Invitrogen) and incubated at 37°C for 8 minutes to obtain a single-cell
452 suspension. Cell debris and large clumps were removed by passing the single-cell suspension through a
453 40 µm filter, followed by centrifugation at 250g for 5 minutes. Prior to nuclei isolation, the cells were
454 washed once with ice-cold PBS supplemented with 0.04% BSA and counted to obtain 1 million cells.
455 Single nuclei were isolated following the protocol for nuclei isolation from fresh cells (Protocol CG000365
456 Rev C, 10X Genomics). Briefly, 100 µl of chilled Lysis Buffer was added to the cell pellet, mixed by
457 pipetting 10 times, incubated for 5 minutes on ice, and washed with 1 ml of Wash Buffer. Nuclei were
458 pelleted by centrifugation at 500g for 5 minutes at 4°C, washed two more times, then resuspended in
459 Nuclei Buffer and immediately processed for sequencing.

460 ### cDNA library preparation and sequencing

461 For single-cell RNA sequencing together with single-cell ATAC sequencing, Multiome 3v3.1 GEX and
462 ATAC libraries were prepared by using the Chromium Next GEM Single Cell Multiome ATAC + Gene
463 Expression Reagent Kits following the recommended protocol (User Guide, CG000338, 10X Genomics).
464 Samples were prepared on the 10x Genomics platform using the Chromium Next GEM Single Cell
465 Multiome ATAC + Gene Expression Reagent Bundle (16 rxns, PN-1000283), Chromium Next GEM Chip J
466 Single Cell Kit (48 rxns, PN-1000234), Single Index Kit N Set A (96 rxns, PN-1000212, for ATAC), and Dual
467 Index Kit TT Set A (96 rxns, PN-1000215, for 3v3.1 GEX). The concentration of each library was
468 determined by qPCR using the KAPA Library Quantification Kit (qPCR MasterMix cat#7959478001, and
469 Library Quantification Kit, Cat# 7960085001, Roche Diagnostics System), following the manufacturer's
470 protocol, to achieve appropriate cluster counts for the Illumina NovaSeq6000 instrument. GEX libraries
471 were pooled and run on 0.0192 of a NovaSeq X Plus 25B flow cell using a 28x10x10x150 sequencing

472 recipe, as per the manufacturer's protocol, with a target coverage of 500M read-pairs per sample. ATAC
473 libraries were pooled and run on 0.0115 of a NovaSeq X Plus 25B flow cell with a 51x8x16x51 sequencing
474 recipe, following the manufacturer's protocol, aiming for a target coverage of 300M read-pairs per
475 sample.
476

477 **Data processing**

478 Single-cell RNA-seq and ATAC-seq data were processed using the 10x Genomics Cell Ranger ARC
479 pipeline (version 2.0.2). For alignment and quantification of gene expression data, raw sequencing reads
480 were processed using the default parameters provided by the 10x Genomics software suite. The
481 standard reference genome and annotations used were based on the refdata-cellranger-arc-GRCh38-
482 2020-A-2.0.0 build provided by 10x Genomics. Briefly, the Illumina sequencer's base call files (BCLs) for
483 each flow cell directory (ATAC or Gene Expression) were demultiplexed using the Illumina bcl2fastq
484 software to generate FASTQ files. These reads were then aligned to the GRCh38 human reference
485 genome, and unique molecular identifier (UMI) counts were obtained using the 10x Cell Ranger toolkit.
486 Barcode selection and filtering for single-cell droplets were performed according to the Cell Ranger
487 pipeline[11,27]

488 **Data filtering and normalization**

489 Single-cell Multiome libraries were used for initial quality control and cell filtering. For the present
490 study, downstream analyses were performed exclusively on the RNA-seq data, which is the focus of this
491 manuscript. Analyses of the ATAC-seq data will be reported separately. UMI count matrices for single
492 cells were analyzed in Seurat (v5.0)[45]. To ensure data quality, cells with fewer than 1,000 RNA counts or
493 more than 25,000 RNA counts were removed, along with cells where more than 50% of reads were
494 mapped to mitochondrial genes, thereby excluding potential low-quality cells, debris, and likely
495 multiplets. To further refine the dataset, doublets were identified and removed using DoubletFinder [85]

496 based on the expected doublet rate and model homotypic interactions, ensuring more accurate cell
497 classification. Following these steps, we applied the SCTransform method, a regularized negative
498 binomial regression approach that corrects for sequencing depth and other technical variations while
499 preserving biological heterogeneity in the dataset[86]. The output from SCTransform was used to identify
500 highly variable features, which were then used for downstream analysis.

501 **Marker gene identification for cell clustering**

502 To identify marker genes across all clusters, we used the FindAllMarkers function in Seurat. Genes
503 were designated as marker genes for a given cluster if they were significantly upregulated in that cluster
504 (Wilcoxon rank-sum test $p < 0.05$), expressed in at least 25% of cells within the cluster, and showed a
505 minimum log fold change of 0.25 (indicating approximately 19% higher expression) relative to other
506 clusters. Expression heatmaps of the top 10 signature genes for each cluster are shown in Figure 3b, and
507 all marker genes names and statistics for their enrichment are provided for every cluster in
508 **Supplementary dataset 1**.

509 **Differential gene expression analysis**

510 To identify gene expression variability and cell-specific responses to treatment, differential gene
511 expression within individual cell clusters was analyzed. Differentially expressed genes (DEGs) were
512 identified using Seurat's FindMarkers function to evaluate transcriptional changes across cell clusters
513 following LT treatment. For each cluster, DEGs were determined using a log2-fold-change threshold of
514 ±0.25 to capture biologically relevant differences, and considering only genes expressed in at least 30%
515 of cells within each group. The Wilcoxon rank-sum test was used for statistical comparisons, allowing
516 identification of both up- and down-regulated genes and providing a comprehensive view of treatment-
517 induced transcriptional changes. The list of all DEGs is provided in **Supplementary dataset 2**.

518 ### Cell cycle analysis

519 Each cell was annotated for its cell cycle stage using the CellCycleScoring function and the updated
520 G1/S and G2/M cell cycle genes from the `cc.genes.updated.2019` dataset in Seurat[46,87], which evaluates
521 the expression of stage-specific marker genes. Specifically, this function assigns each cell a quantitative
522 score based on the expression of 54 genes related to the S phase and 43 genes associated with the G2/M
523 phase[27106]. By comparing these scores, cells were categorized as being in G1, S, or G2/M phases. Cells
524 with low scores in both S and G2/M markers are inferred to be in the G1 phase, indicating a quiescent or
525 resting state, while cells with high S or G2/M scores are identified as actively cycling. Composition of cell
526 cycle phase across different clusters is provided in supplementary source data for tables (see
527 Supplementary table 4). For visualization, the distribution of cell cycle phases per sample and cluster was
528 plotted using ggplot2.

529 ### Labeling of proliferating cells

530 Actively proliferating cells were detected using the Click-iT EdU imaging kit (Molecular Probes, Life
531 Technologies) according to the manufacturer's protocol. Briefly, following toxin treatments, organoids
532 were incubated for three hours at 37°C in tissue culture media supplemented with 10 µM EdU. Following
533 incubation, organoids were fixed with 4% paraformaldehyde as previously described and permeabilized
534 with 0.5% Triton X-100 for 20 minutes at room temperature. The EdU-labeled cells were detected with
535 the Click-iT® Plus reaction cocktail, followed by counterstaining with DAPI. For EdU analysis, twenty
536 random fields were imaged at 20× magnification, and the numbers of EdU-positive and DAPI-positive
537 nuclei were counted. The percentage of EdU-positive nuclei was calculated as a proportion of the total
538 nuclei count per enteroid. Each experiment was conducted in duplicate.

539 ### Functional enrichment analysis

540 Ontology-independent algorithms in CompBio 2.9 (COmprehensive Multi-omics Platform for
541 Biological InterpretatiOn) (https://gtac.wustl.edu/bioinformatics/) were used to analyze existing

542 transcriptome data in RNAseq datasets. Enrichment analysis was carried out using WebGestalt
543 (https://www.webgestalt.org/) against reference gene sets curated from Reactome pathways and
544 network databases. Over-representation analysis (ORA) was performed to identify biological pathways
545 and functional categories significantly enriched among differentially expressed genes. Genes with an
546 adjusted *p*-value < 0.05 were selected as input. Statistical significance was determined using a
547 hypergeometric test, with p-values adjusted for multiple testing by the Benjamini–Hochberg method
548 (FDR < 0.05). Redundancy among enriched categories was reduced using the weighted set cover method,
549 and results were visualized to highlight key biological processes associated with the gene sets.

550 **Statistical analysis**

551 All statistical analyses were conducted using GraphPad Prism (version 10.5.0) and RStudio (version
552 2023.12.1), unless otherwise specified. For comparisons between two groups, the non-parametric
553 Mann–Whitney U test was used. For comparisons among more than two groups, the Kruskal–Wallis test
554 followed by Dunn's multiple comparisons test was applied. To assess differences in cell proportions or
555 categorical distributions across experimental conditions, Chi-square (χ^2) tests were used. When
556 applicable, exact *P*-values were calculated and reported. In figures, statistical significance is indicated as:
557 P < 0.05 (*), P < 0.01 (**), P < 0.001 (***), and P < 0.0001 (****).
558

559 **Data availability**

560 Single-cell RNA-seq data have been deposited in the NCBI Sequence Read Archive (SRA) under the
561 BioProject accession PRJNA1330728 (https://www.ncbi.nlm.nih.gov/bioproject/). Primary source data
562 and original images are available on Figshare, as detailed in Supplementary table 4. All other data
563 supporting the findings of these studies are included in the manuscript as supplementary dataset and
564 are also available from the corresponding author upon reasonable request.
565

566 ## Figures

567 ### Figure 1

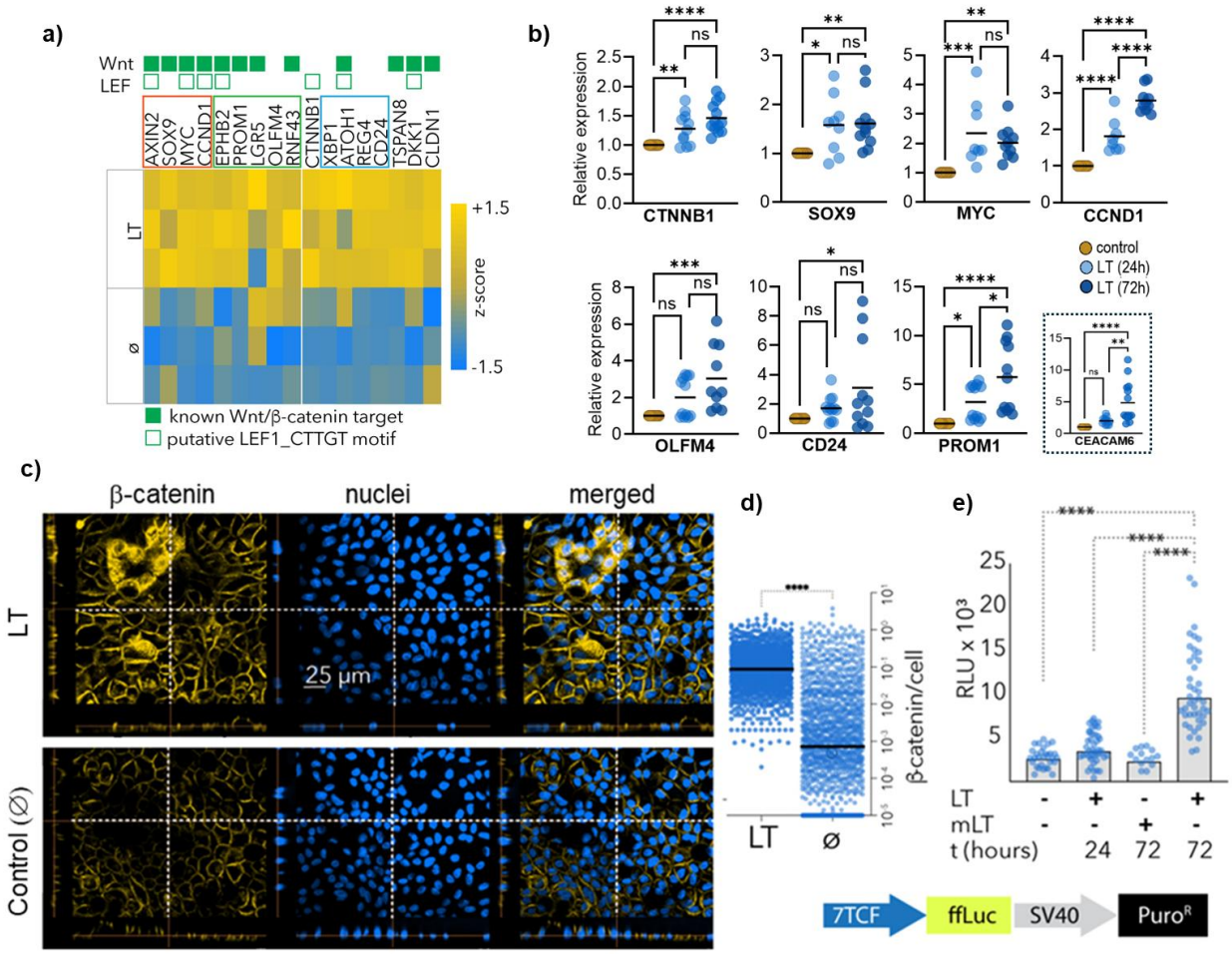

568

569

570 **Figure 1. LT activates WNT/β-catenin signaling in human intestinal epithelial cells.**

571 **a**) Heatmap showing differential expression (z-score) of WNT/β-catenin signaling components and target

572 genes in control (Ø) and LT-treated enteroids based on bulk RNA-seq. Closed green symbols signify genes

573 known to be modulated by canonical WNT-β-catenin pathway as profiled

574 (https://web.stanford.edu/group/nusselab/cgi-bin/wnt/target_genes). Open green symbols indicate

575 genes possessing an upstream 3'UTR CTTTGT motif for the LEF1: lymphoid enhancer-binding factor

576 http://www2.stat.duke.edu/~sayan/genesets/Jan2006/cards/C3/CTTTGT_V_LEF1_Q2.html. **b**) RT-qPCR

validation of selected genes showing significantly increased expression following LT treatment. Gene expression was measured at 24 and 72 hours post-treatment. Data are presented as expression levels normalized to GAPDH and shown relative to the untreated control. Inset: CEACAM6 expression is included as a positive control for LT-mediated induction. Statistical comparisons were made using Kruskal-Wallis; ns = not significant, *$p < 0.05$, **$p < 0.01$, ***$p < 0.001$, ****$p < 0.0001$. **c**) Representative confocal immunofluorescence images of β-catenin (yellow) and nuclei (blue) in LT-treated and control enteroids showing increased nuclear β-catenin accumulation in LT-treated samples. Scale bar, 25 µm. **d**) Quantification of nuclear β-catenin intensity per cell from images shown in panel (c). Each dot represents an individual nucleus. ****$p<0.0001$ Mann-Whitney (two-tailed). **e**) Luciferase reporter activity (in Relative light units, RLU) following treatment of Hu235D::7TFP cells with heat-labile toxin (LT) or mutant, catalytically inactive toxin (mLT, E112K). The data shown are combined from 3-7 independent experiments. Each dot represents signal per well and each Bar represents geometric mean. Statistical analysis by one-way ANOVA (Kruskal-Wallis), ****$p<0.0001$.

592 **Figure 2**

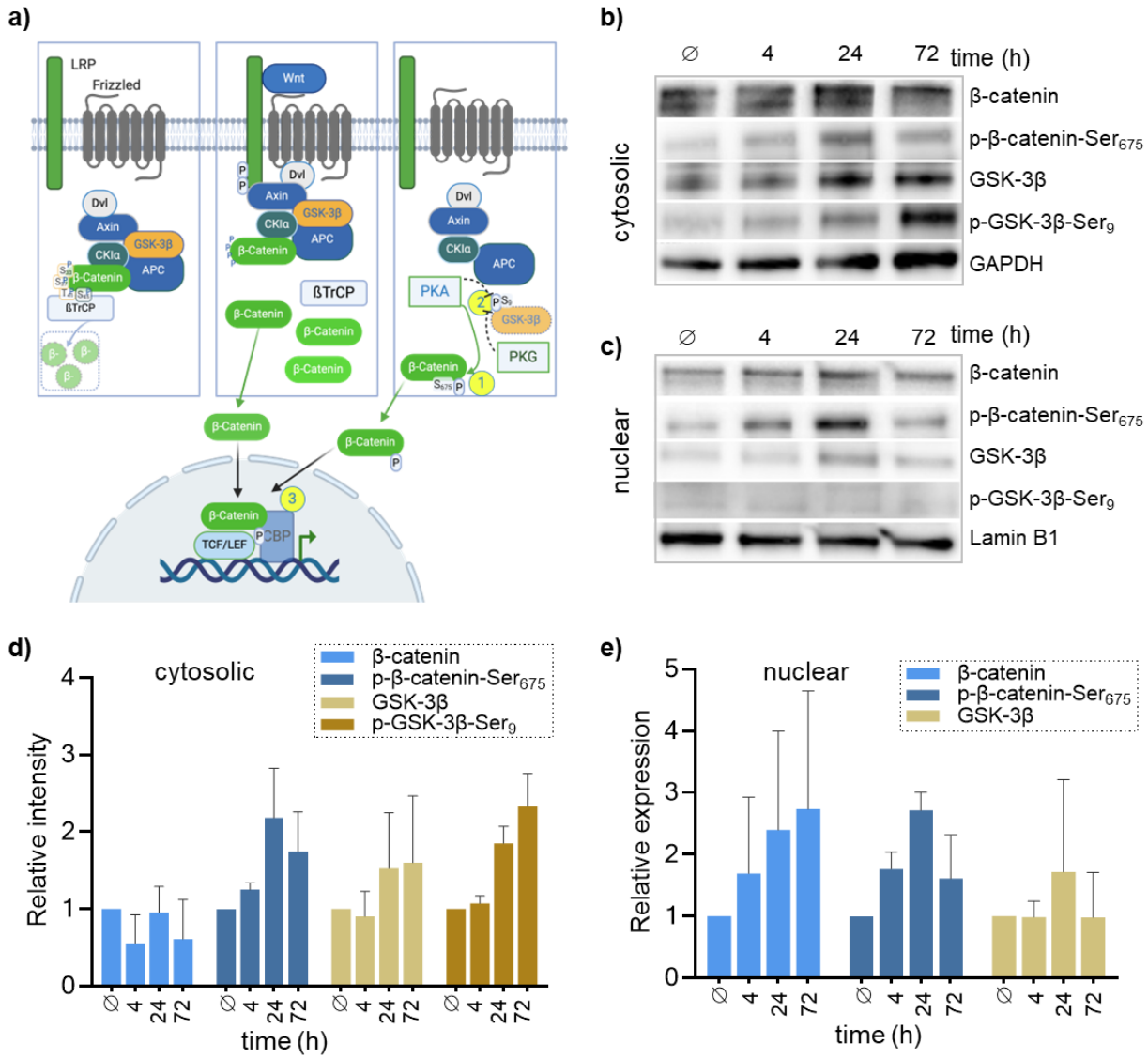

593

594 **Figure 2. Heat-labile toxin stabilizes β-catenin signaling independent of WNT.**

595 **a)** Diagram illustrating canonical WNT–β-catenin signaling (left and middle panels). Panel at right

596 depicts anticipated impacts of PKA-mediated, WNT-independent signaling. **b**) Representative

597 immunoblots of cytoplasmic and **c**) nuclear fractions from LT-treated enteroids at indicated time points

598 (4, 24, 72 hours) or untreated controls (Ø). Blots were probed for total β-catenin, phospho-β-catenin

599 (Ser_{675}), total GSK3β, and phospho-GSK3β (Ser_9). GAPDH and lamin B1 served as loading controls for

600 cytoplasmic and nuclear fractions, respectively. **d-e)** Graphs represent densitometry measurements of

601 immunoblots of cytoplasmic (**d**) and nuclear (**e**) fractions, normalized to respective loading controls,

602 summarizing 4 independent experiments. Bars represent geometric means ± SD.

603

604 **Figure 3**

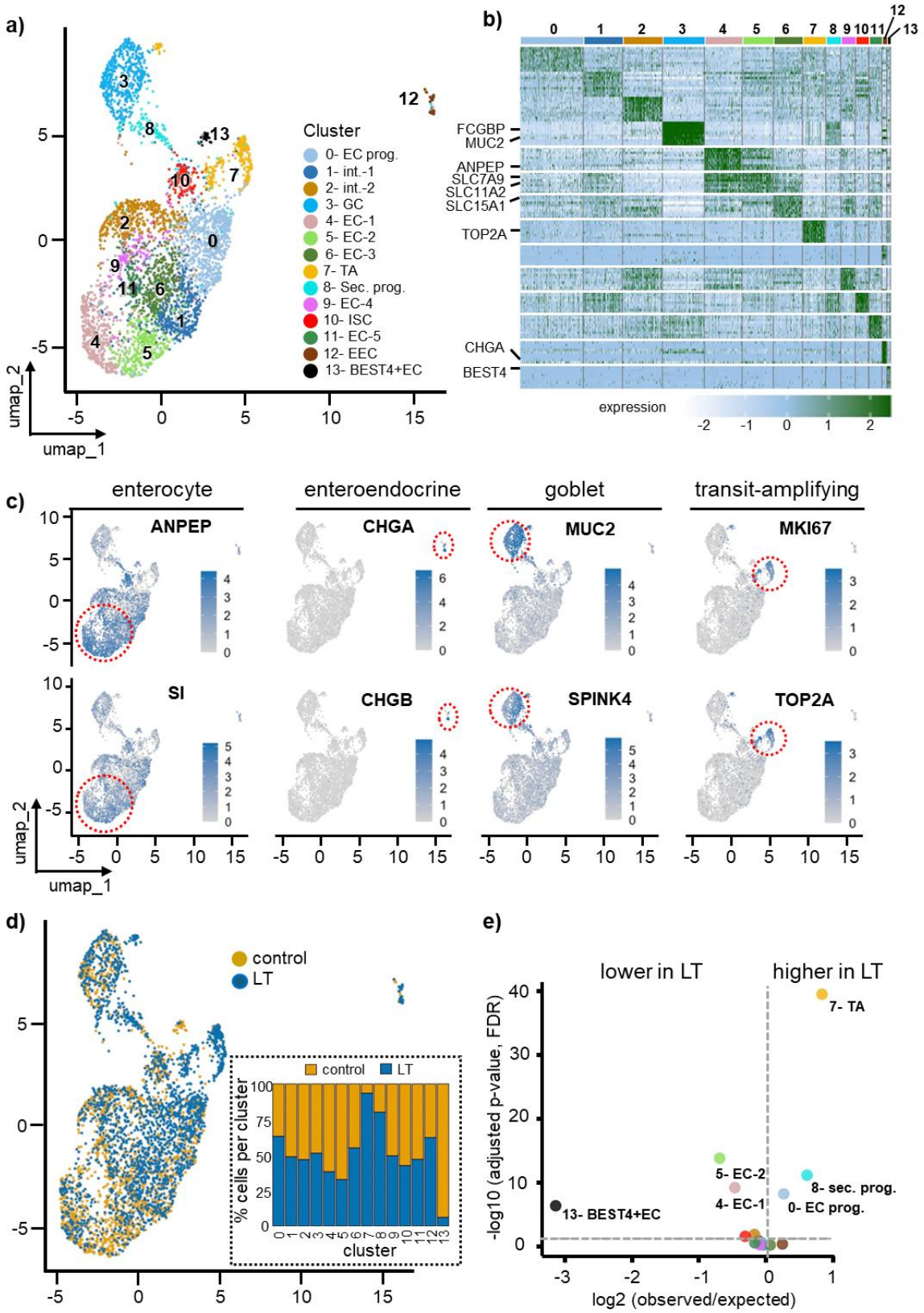

605

606 **Figure 3. LT treatment reshapes intestinal epithelial cell composition**.

607 **a**) UMAP projection of single-cell transcriptomes from control and LT-treated ileal enteroids, colored
608 by cluster identity. Unsupervised clustering identified 14 transcriptionally distinct epithelial populations,
609 which were annotated based on lineage marker gene expression. These include enterocyte progenitors,
610 intermediate cells, secretory lineages (goblet, enteroendocrine, and Paneth-like), stem cells, and
611 multiple stages of differentiated enterocytes. **b**) Heatmap showing the relative expression levels of the
612 top 10 marker genes per cluster, showing distinct transcriptional signatures corresponding to absorptive,
613 secretory, intermediate, and proliferative compartments. Expression values represent SCTransform-
614 normalized Pearson residuals. **c**) UMAP feature plots showing expression of known cell type specific
615 markers. Enterocyte markers: ANPEP, SI, ALPI; goblet cell markers: MUC2, SPINK4, TFF3; enteroendocrine
616 cell markers: CHGA, CHGB, THP1; transit-amplifying cell markers: MKI67, TOP2A, PCNA. Red dotted
617 circles highlight specific cell clusters with high expression values. **d**) UMAP showing the distribution of
618 cells from control (orange) and LT-treated (blue) samples, revealing a shift in cell type representation.
619 Inset: Stacked bar plot showing the proportion of cells from each sample (control vs LT) within each
620 cluster. **e**) Differential abundance analysis for epithelial cell clusters in LT-treated versus control
621 enteroids. Each point represents an epithelial cell cluster. The x-axis shows the $\log_2$ ratio of observed to
622 expected cell counts in LT-treated enteroids, and the y-axis shows the $-\log_{10}$(FDR-adjusted p-value).
623 Vertical and horizontal dashed lines indicate the direction of change (assigned based on whether the
624 observed LT count exceeded or fell below the expected value) and statistical significance thresholds,
625 respectively. Clusters to the right of the vertical line are enriched in LT-treated samples, whereas clusters
626 to the left are reduced. Significantly altered clusters are labeled. Statistical analysis was performed per
627 cluster using a Chi-square test with FDR correction (significant if FDR <0.05). BEST4+EC, BEST4 positive
628 enterocyte; EC, enterocyte; EC prog.- enterocyte progenitor; EEC, enteroendocrine cell; GC, goblet cell;
629 ISC, intestinal stem cell; int., intermediate; sec. prog., secretory progenitor; TA, transit amplifying.

630 **Figure 4**

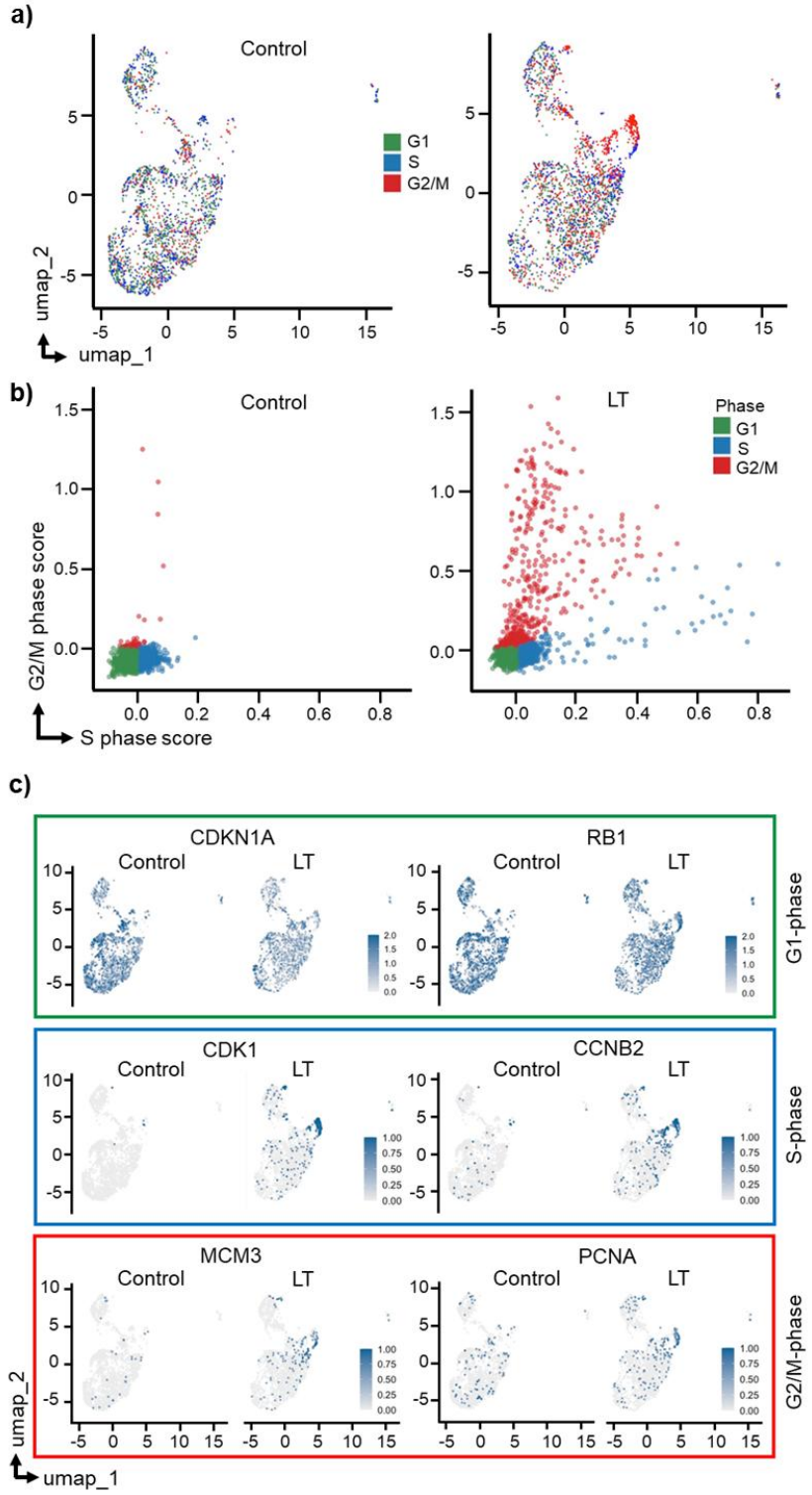

631
632
633 **Figure 4: LT alters epithelial cell cycle dynamics.**

634 **a**) UMAP projections of single-cell transcriptomes from control and LT-treated human ileal enteroids,
635 colored by assigned cell cycle phase based on canonical marker gene expression (G1, S, G2/M). **b**) XY
636 scatterplots of individual cell S-phase and G2/M-phase scores derived from gene expression signatures.
637 **c**) UMAP feature plots highlighting expression of representative phase-specific marker genes across
638 conditions. G1-associated genes (RB1, CDKN1A), S-phase associated genes (PCNA, MCM3) and G2/M-
639 phase associated genes (CCNB2, CDK1). Color scales represent normalized expression.
640

641 **Figure 5**

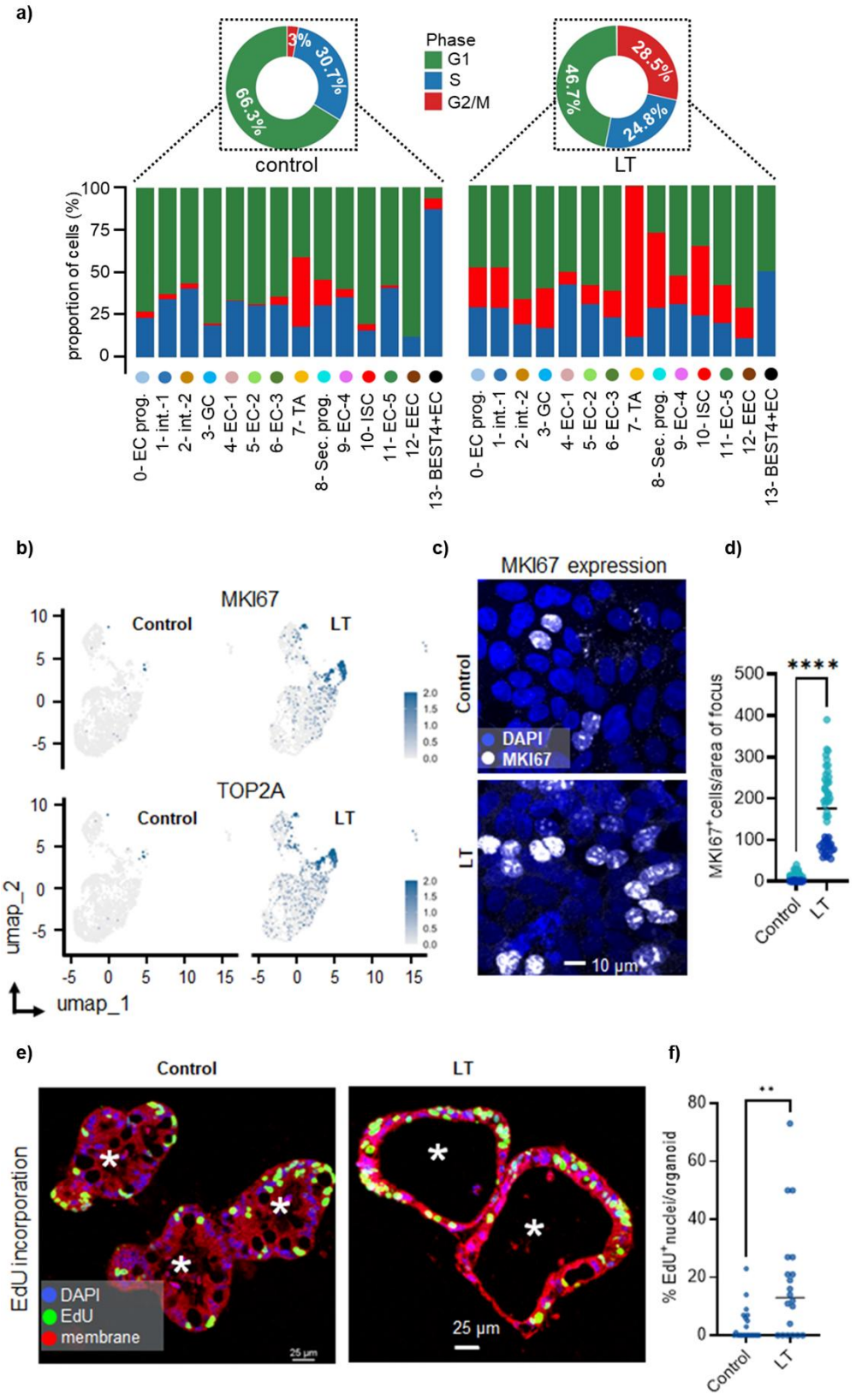

642

Figure 5: LT affects cell cycle progression across intestinal epithelial lineages and promotes epithelial proliferation.

a) Donut charts represent the global distribution of cells across cell cycle phases in control and LT-treated enteroids. Bar plots below show the proportion of cells in G1 (green), S (blue), and G2/M (red) phases across transcriptionally defined cell clusters (0–13) in control and LT-treated enteroids. **b**) UMAP feature plots showing expression of proliferation markers MKI67 (top) and TOP2A (bottom) in control (left) and LT-treated (right) human ileal enteroids. The color scale indicates normalized expression levels. **c**) Representative confocal images of MKI67 (white) and nuclei (DAPI, blue) in control (left) and LT-treated (right) enteroids. Scale bar, 10 µm. **d**) Quantification of $MKI67^+$ cells per field of view. Each point represents the number of $MKI67^+$ nuclei in an individual field; the horizontal line denotes the mean. Data are from two independent experiments (≥50 fields of view total). Statistical significance was determined by a two-tailed, nonparametric Mann–Whitney test (****$p < 0.0001$). **e**) Representative confocal images of control (left) and LT-treated (right) enteroids labeled with EdU (green) for DNA synthesis, DAPI (blue) for nuclei, and a membrane stain (red). White asterisks mark the luminal space (equivalent to intestinal lumen) in enteroids. Off note, LT-treated enteroids showed a marked increase in luminal area, consistent with LT-induced fluid secretion. Scale bar, 25 µm. **f**) Quantification of EdU^+ nuclei per enteroid (n = 25 enteroids per treatment). Each point represents the number of EdU^+ nuclei per individual enteroid; the horizontal line denotes the mean. Statistical significance was determined by a two-tailed, nonparametric Mann–Whitney test (**$p < 0.01$).

662 **Figure 6**

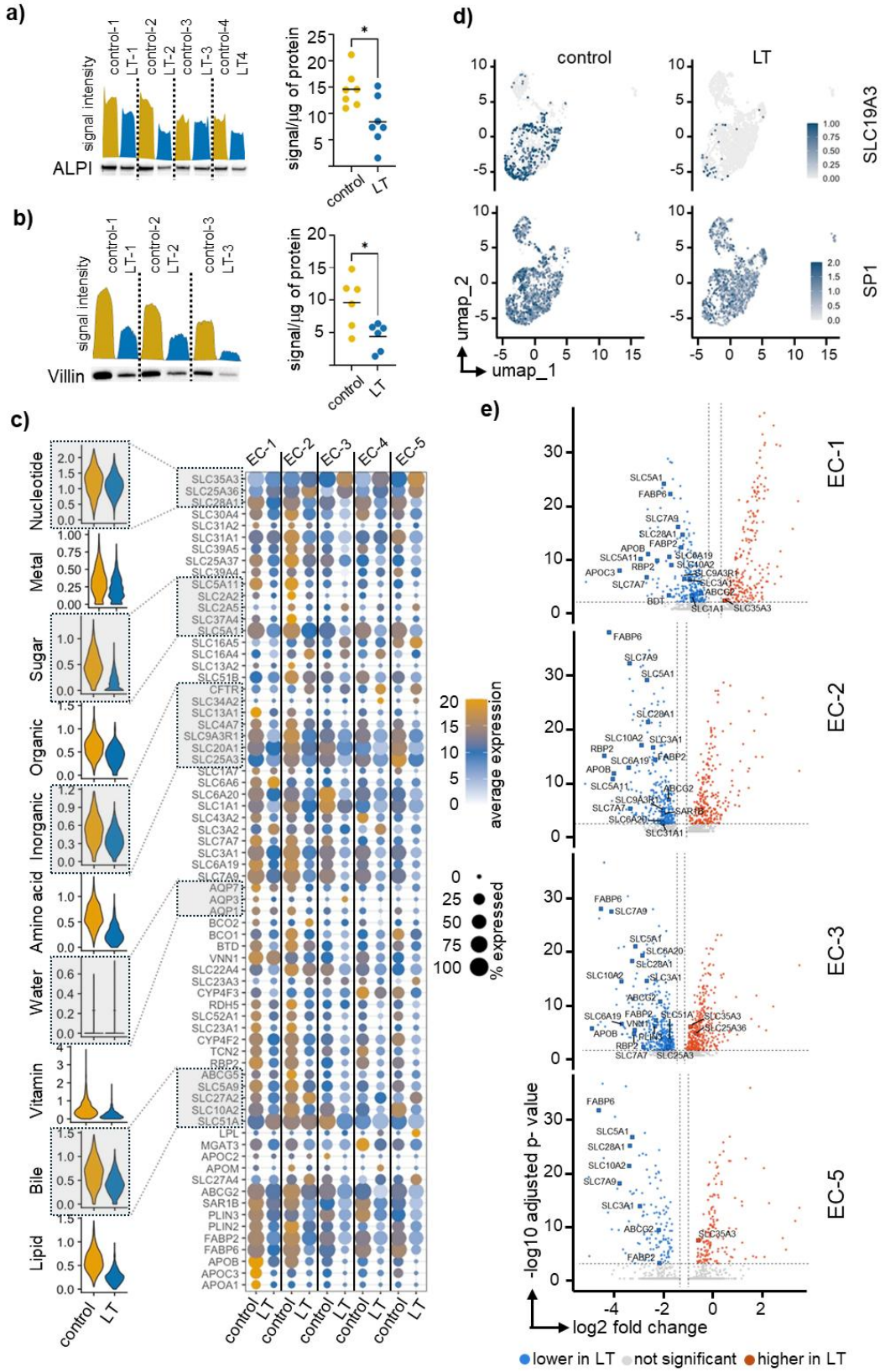

663

664 **Figure 6. LT affects enterocyte maturation and disrupts nutrient transporter expression.**

665 **a**) Western blot analysis of ALPI (intestinal alkaline phosphatase enzyme) expression in control and LT-
666 treated enteroids. Representative blot and corresponding densitometric histograms generated using
667 ImageJ (left). Quantification of normalized ALPI expression (right). Each data point represents an
668 individual replicate (n = 7 per group). Horizontal lines on the plot indicate mean. Statistical significance
669 was determined using a non-parametric Mann-Whitney test (*$p < 0.05$, two-tailed). **b**) Western blot
670 analysis of Villin (structural protein) expression in control and LT-treated enteroids. Representative blot
671 and corresponding densitometric histograms generated using ImageJ (left). Quantification of normalized
672 Villin expression (right). Each data point represents an individual replicate (n = 6 per group). Horizontal
673 lines on the plot indicate mean. Statistical significance was determined using a non-parametric Mann-
674 Whitney test (*$p < 0.05$, two-tailed). **c**) Analysis of nutrient transporter genes across enterocyte
675 subclusters (EC-1 to EC-5). Data were derived from scRNA-seq of control and LT-treated enteroids. Violin
676 plots showing distributions of mean expression of major nutrient transporter gene families (nucleotide,
677 metal, sugar, organic, inorganic, amino acid, water, vitamin, bile, lipid). Dot plot illustrating expression
678 patterns of specific genes involved in nutrient absorption and transport. The color scale indicates the
679 average expression, and the dot size indicates proportion of cells expressing individual transporter genes
680 across five enterocyte subclusters (EC-1 to EC-5). **d**) UMAP feature plots showing SLC19A3 thiamine
681 transporter and SP1 regulator gene expression across cell clusters. **e**) Volcano plots showing differential
682 expression of nutrient transporter genes within enterocyte subclusters EC-1 through EC-5. The x-axis
683 indicates $\log_2$ fold-change (LT vs. control), and the y-axis indicates $-\log_{10}$ adjusted p-value. Genes
684 significantly upregulated in LT-treated enteroids are shown in red, significantly downregulated genes in
685 blue, and non-significant changes in gray. Selected transporters with significant changes are labeled.
686 Statistical testing was performed using a Wilcoxon rank-sum test with Benjamini–Hochberg correction for
687 multiple comparisons; adjusted $p < 0.05$ was considered significant. EC, enterocyte.

688 **Tables**

689 **Table-1. Transcriptionally-defined epithelial cell cluster compositions in ileal enteroids.**

Cluster	Identity		Treatment conditions		Chi2 Statistic	*P* Value	Change with LT
			Control (%)	LT (%)			
0	EC prog.	Enterocyte progenitor	270 (13.8)	461 (20.9)	36.079	1.90E-09	Expanded
1	int.-1	Intermediate-1	229 (11.7)	217 (9.8)	3.467	6.26E-02	Not Significant
2	int. -2	Intermediate-2	242 (12.3)	212 (9.6)	7.658	5.65E-03	Depleted
3	GC	Goblet cell	234 (11.9)	246 (11.1)	0.538	4.63E-01	Not Significant
4	EC-1	Enterocyte-1	264 (13.4)	163 (7.4)	40.897	1.60E-10	Depleted
5	EC-2	Enterocyte-2	239 (12.2)	116 (5.3)	62.978	2.09E-15	Depleted
6	EC-3	Enterocyte-3	147 (7.5)	179 (8.1)	0.475	4.91E-01	Not Significant
7	TA	Transit amplifying	17 (0.9)	243 (11.0)	181.147	2.72E-41	Expanded
8	Sec. prog.	Secretory progenitor	33 (1.7)	133 (6.0)	50.188	1.40E-12	Expanded
9	EC-4	Enterocyte-4	80 (4.1)	78 (3.5)	0.693	4.05E-01	Not Significant
10	ISC	Intestinal stem cell	84 (4.3)	62 (2.8)	6.216	1.27E-02	Depleted
11	EC-5	Enterocyte-5	76 (3.9)	67 (3.0)	1.947	1.63E-01	Not Significant
12	EEC	Enteroendocrine cell	17 (0.9)	28 (1.3)	1.223	2.69E-01	Not Significant
13	BEST4+EC	BEST4+ enterocyte	31 (1.6)	2 (0.1)	27.458	1.61E-07	Depleted

690

691

692 **Table-2. Total number of differentially expressed genes per cluster following LT treatment**

Description		Cell counts		Number of differentially expressed genes (DEGs)*	
Cluster #	**Identity**	**control**	**LT**	**Higher in LT**	**Lower in LT**
0	Enterocyte progenitor	270	461	634	901
1	Intermediate-1	229	217	455	545
2	Intermediate-2	242	212	447	323
3	Goblet cell	234	246	236	509
4	Enterocyte-1	264	163	256	274
5	Enterocyte-2	239	116	310	310
6	Enterocyte-3	147	179	354	420
7	Transit amplifying	17	243	N/A	N/A
8	Secretory progenitor	33	133	85	305
9	Enterocyte-4	80	78	N/A	N/A
10	Intestinal stem cell	84	62	157	267
11	Enterocyte-5	76	67	148	132
12	Enteroendocrine cell	17	28	N/A	N/A
13	BEST4+ enterocyte	31	2	N/A	N/A

* Differentially expressed genes across epithelial clusters in LT-treated vs. control enteroids. Genes with minimal log2FC of +/-0.25, and expressed in at least 10% of cells with FDR adjusted P value of <0.05 were considered significant.

693

694

695 **Table-3. Cell cycle phase distribution in control and LT-treated enteroids**

Clusters	Phase	Cell count (%)		Chi²_statistic	P value
		Control	LT		
all combined	G1	1303 (66.4)	1031 (46.8)	162.2	< 1e-16
	S	602 (33.7)	546 (24.7)	18	2.21E-05
	G2/M	58 (2.9)	630 (28.5)	492.01	< 1e-16
#0	G1	197 (73.0)	221 (47.9)	61.06	<0.00001
	G2M	10 (3.7)	107 (23.2)		
	S	63 (23.3)	133 (28.9)		
#1	G1	144 (62.9)	104 (47.9)	43.74	<0.00001
	G2M	6 (2.6)	51 (23.5)		
	S	79 (34.5)	62 (28.6)		
#2	G1	137 (56.6)	139 (65.6)	37.596	<0.00001
	G2M	7 (2.9)	32 (15.1)		
	S	98 (40.5)	41 (19.3)		
#3	G1	187 (79.9)	147 (59.8)	53.1702	<0.00001
	G2M	3 (1.3)	57 (23.2)		
	S	44 (18.8)	42 (17.1)		
#4	G1	176 (66.7)	82 (50.3)	23.0313	<0.00001
	G2M	1 (0.4)	12 (7.4)		
	S	87 (33.0)	69 (42.3)		
#5	G1	165 (69.0)	67 (57.8)	21.4174	0.000022
	G2M	2 (0.8)	13 (11.2)		
	S	72 (30.1)	36 (31.0)		
#6	G1	95 (64.6)	110 (61.5)	10.847	0.004412
	G2M	7 (4.8)	28 (15.6)		
	S	45 (30.6)	41 (22.9)		
#7	G1	7 (41.2)	1 (0.4)	90.4198	<0.00001
	G2M	7 (41.2)	214 (88.1)		
	S	3 (17.6)	28 (11.5)		
#8	G1	18 (54.5)	37 (27.8)	11.3691	0.0034
	G2M	5 (15.2)	58 (43.6)		
	S	10 (30.3)	38 (28.6)		
#9	G1	48 (60.0)	41 (52.6)	5.5985	0.061
	G2M	4 (5.0)	13 (16.7)		
	S	28 (35.0)	24 (30.8)		
#10	G1	68 (81.0)	22 (35.5)	38.4988	<0.00001
	G2M	3 (3.6)	25 (40.3)		
	S	13 (15.5)	15 (24.2)		
#11	G1	44 (57.9)	39 (58.2)	19.4254	0.000061
	G2M	1 (1.3)	15 (22.4)		
	S	31 (40.8)	13 (19.4)		
#12	G1	15 (88.2)	20 (71.4)	1.4768	0.47787
	S	NF*	5 (17.9)		
	G1	2 (11.8)	3 (10.7)		
#13	G1	2 (6.5)	1 (50.0)	5.4403	0.065863
	G2M	2 (6.5)	NF*		
	S	27 (87.1)	1 (50.0)		

696 *NF-not found

697

Supplementary data

Supplementary figures

Supplementary figure 1

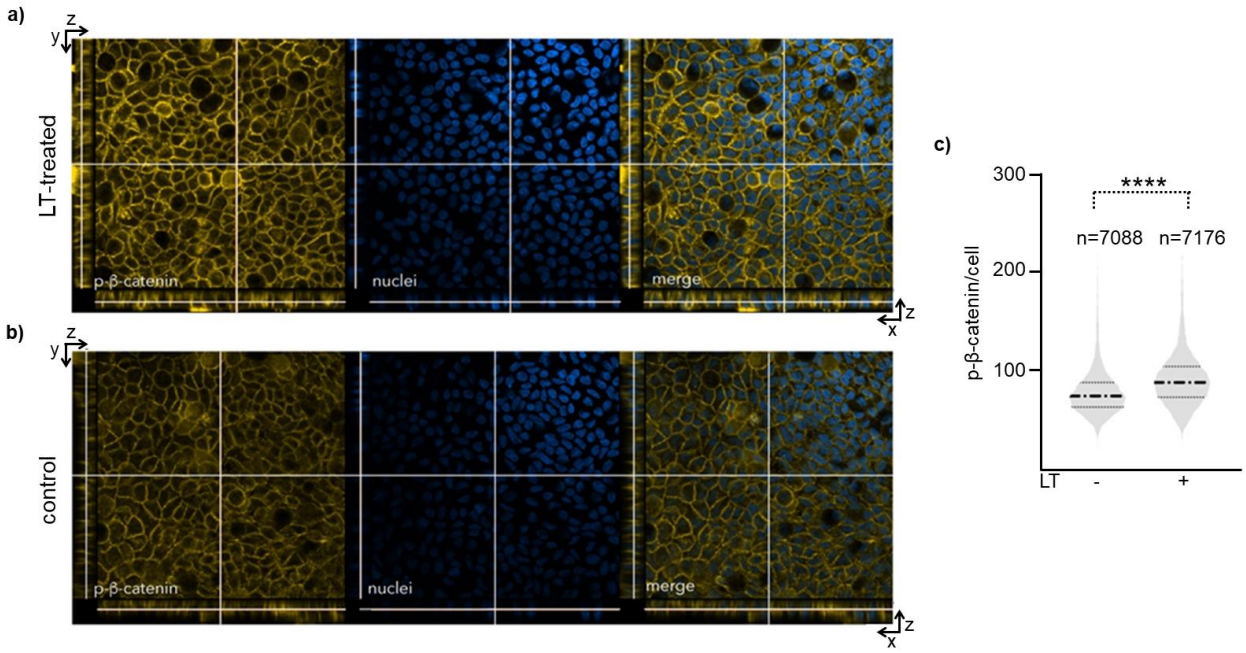

Supplementary figure 1. Phophorylated β-catenin (Ser_{675}) accumulates in target intestinal cells following treatment with heat-labile toxin.

a. Top panels show phospho-β-catenin accumulation in representative field of LT-treated Hu235D cells compared to untreated cells (**b**). **c.** Violin plots at right summarize p-β-catenin Ser_{675} signal per cell obtained from n=7088 cells in control, and n=7176 cells in LT-treated group. Data was accumulated over 20 randomly selected fields. Heavy dashed lines in each group represent median values, thin lines are quartiles. ****$p<0.0001$ (Mann-Whitney).

Supplementary figure 2

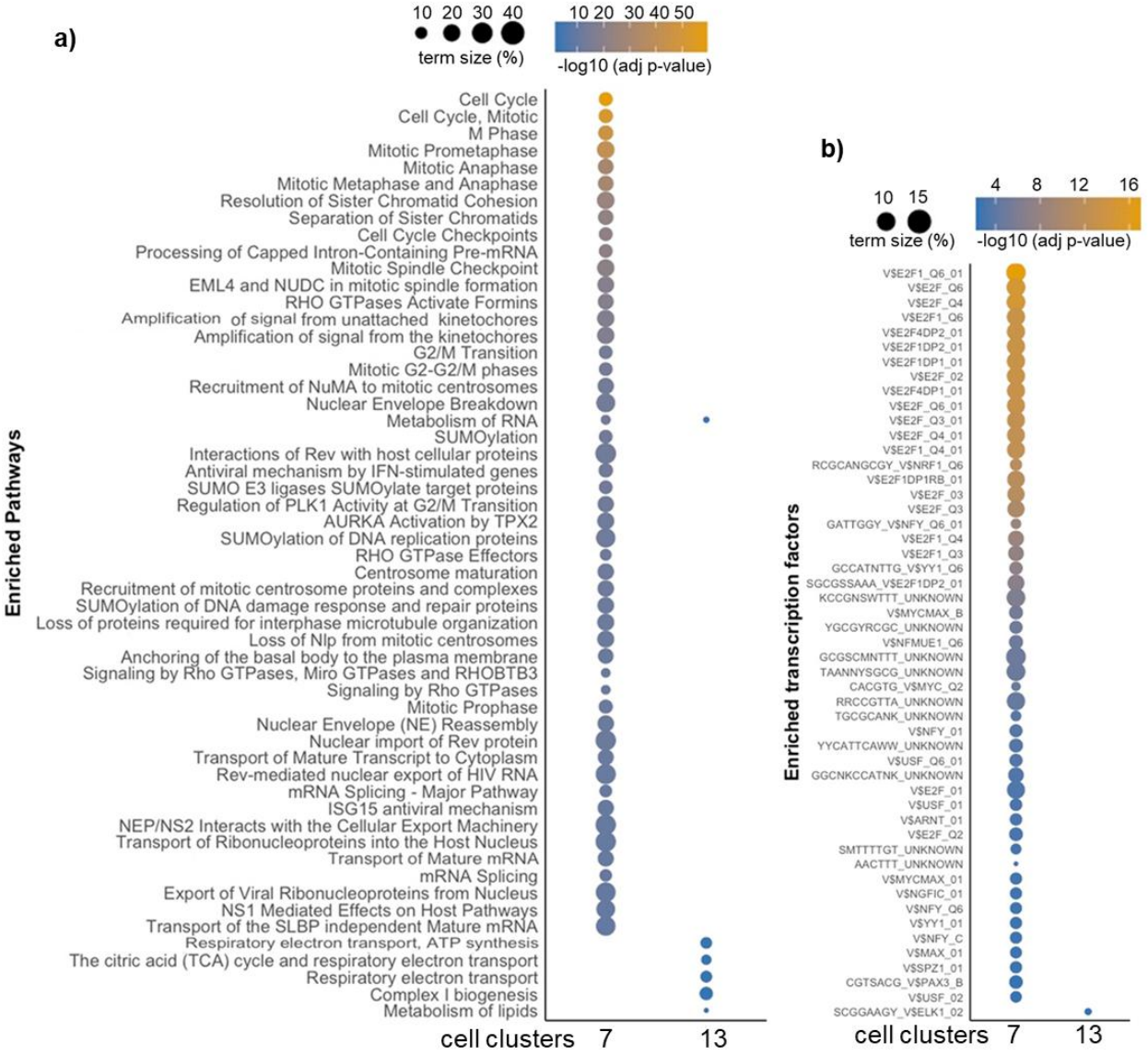

Supplementary figure 2. Over-representation analysis (ORA) of cluster 7 (TA) and cluster 13 marker genes (BEST4+EC). Dot plots displaying significantly enriched (FDR < 0.05) pathways (a) and transcription factors (b) along the Y-axis, among cluster marker genes for clusters 7 and 13. Dot size indicates the number of marker genes contributing to each pathway, and color reflects the adjusted statistical significance (−log10 FDR), with yellow indicating stronger enrichment and blue indicating lower significance.

Supplementary figure 3

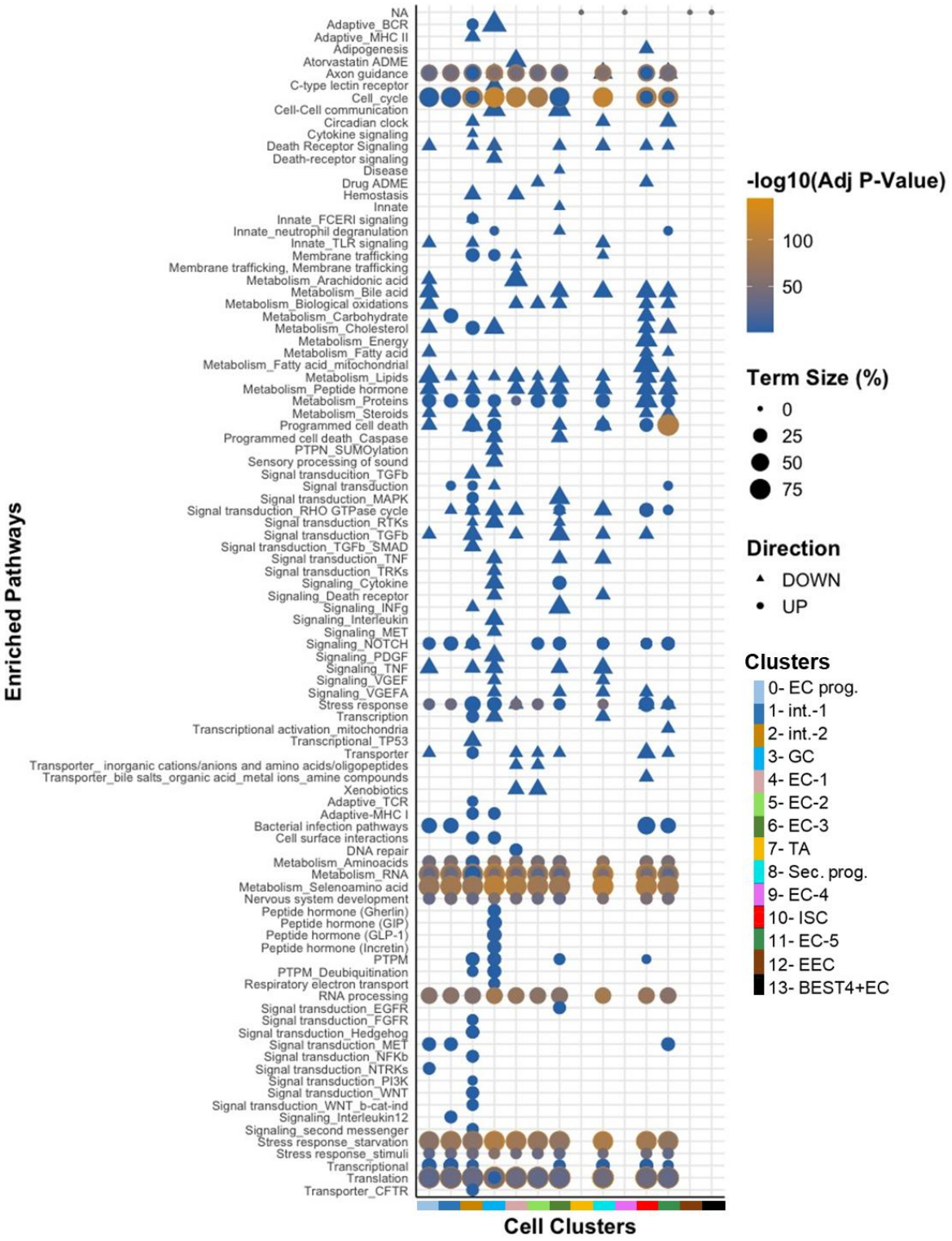

721 **Supplementary figure 3. Over-representation analysis (ORA) of significantly up- and down-**
722 **regulated genes between LT and control samples.**
723 The dot plot displays significantly enriched biological pathways (Y-axis) across 14 epithelial cell
724 clusters (X-axis) among differentially expressed genes in LT-treated vs. control intestinal organoids (FDR
725 <0.05). Circles represent upregulated pathways, while triangles represent downregulated pathways. Dot
726 size indicates the number of DEGs contributing to each pathway, and color reflects the adjusted
727 statistical significance (−log10 FDR), with yellow indicating stronger enrichment and blue indicating lower
728 significance.
729

730 **Supplementary figure 4**

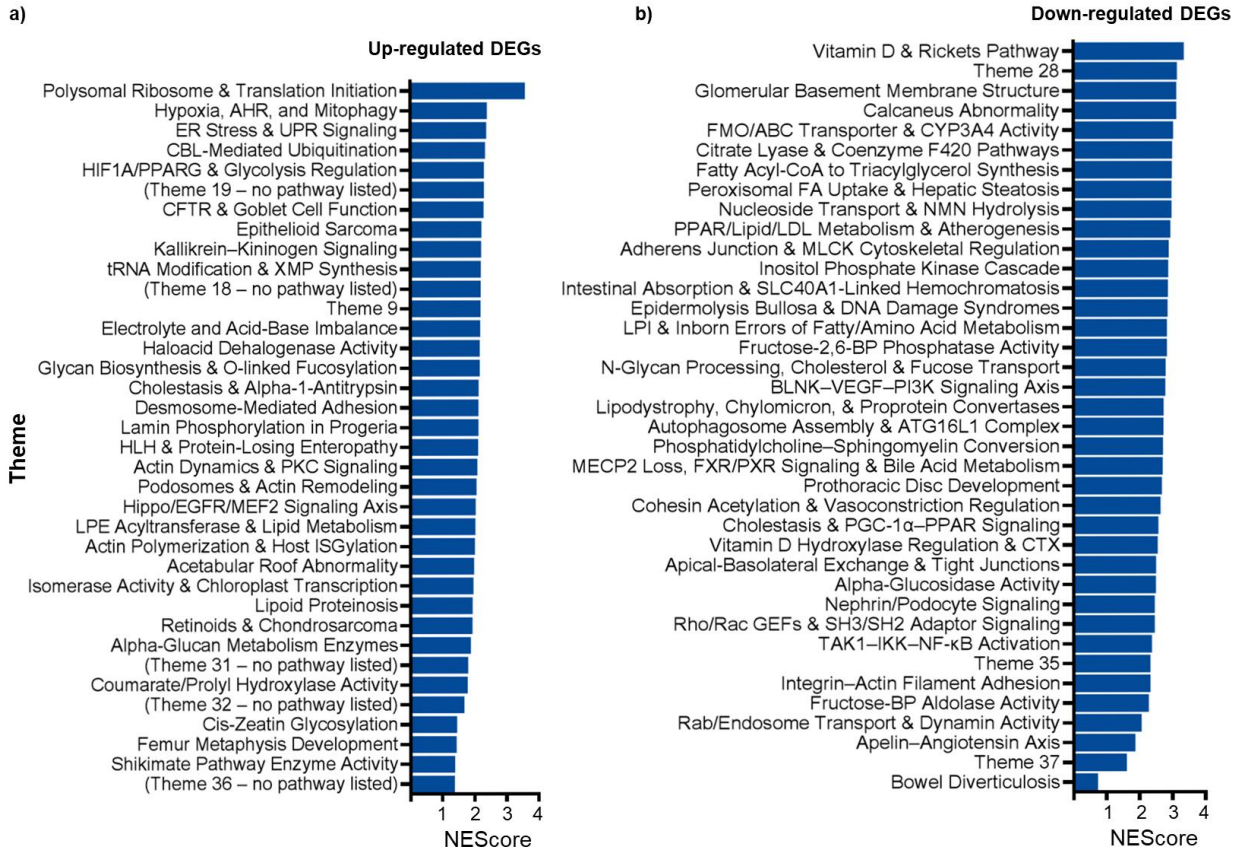

731
732 **Supplementary figure 4. CompBio analysis of differentially expressed genes (DEGs) in LT-treated**

733 **enteroids.**

734 a) Bar plot showing themes significantly enriched among downregulated genes (FDR-adjusted $p < 0.05$).

735 b) Bar plot showing themes significantly enriched among upregulated genes (FDR-adjusted $p < 0.05$).

736 Pathway enrichment was conducted using CompBio v2.9 with default parameters. NEScore represents

737 the normalized enrichment score derived from CompBio theme association analysis. Themes were

738 prioritized based on total score. See Supplementary dataset for full theme descriptions and gene lists.

739 **Supplementary figure 5**

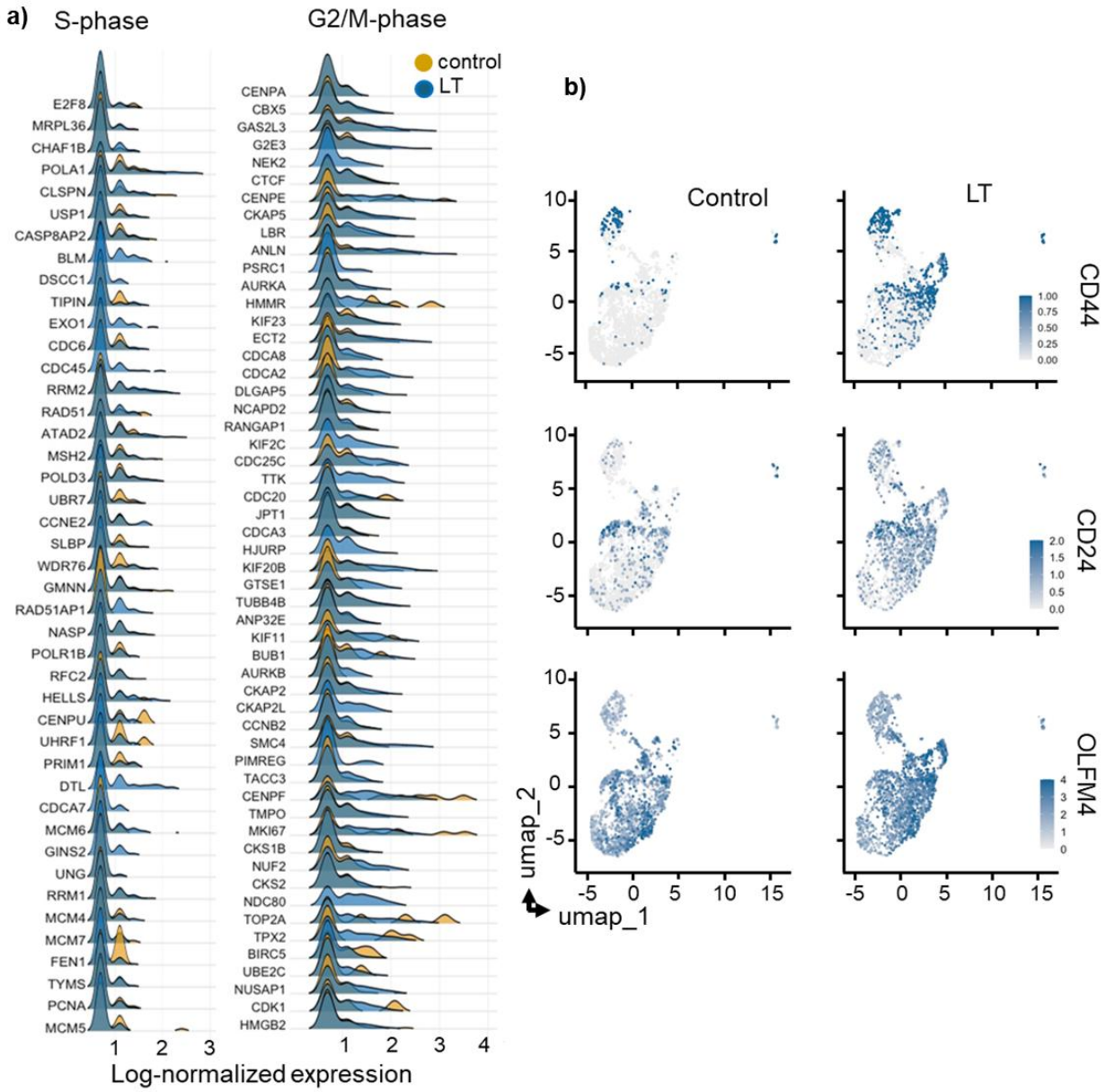

740

741 **Supplementary figure 5: Expression of cell-cycle phase and stem/progenitor genes.**

742 a) Ridge plots showing expression of cell cycle phase marker genes. Normalized expression of S-phase
743 genes (left) and G2/M-phase genes (right) in control and LT-treated enteroids. b) Feature plots displaying
744 expression of CD44, CD24, and OLFM4 markers of stem or undifferentiated states across cell clusters in
745 control (left) and LT-treated (right) enteroids.

746 **Supplementary figure 6**

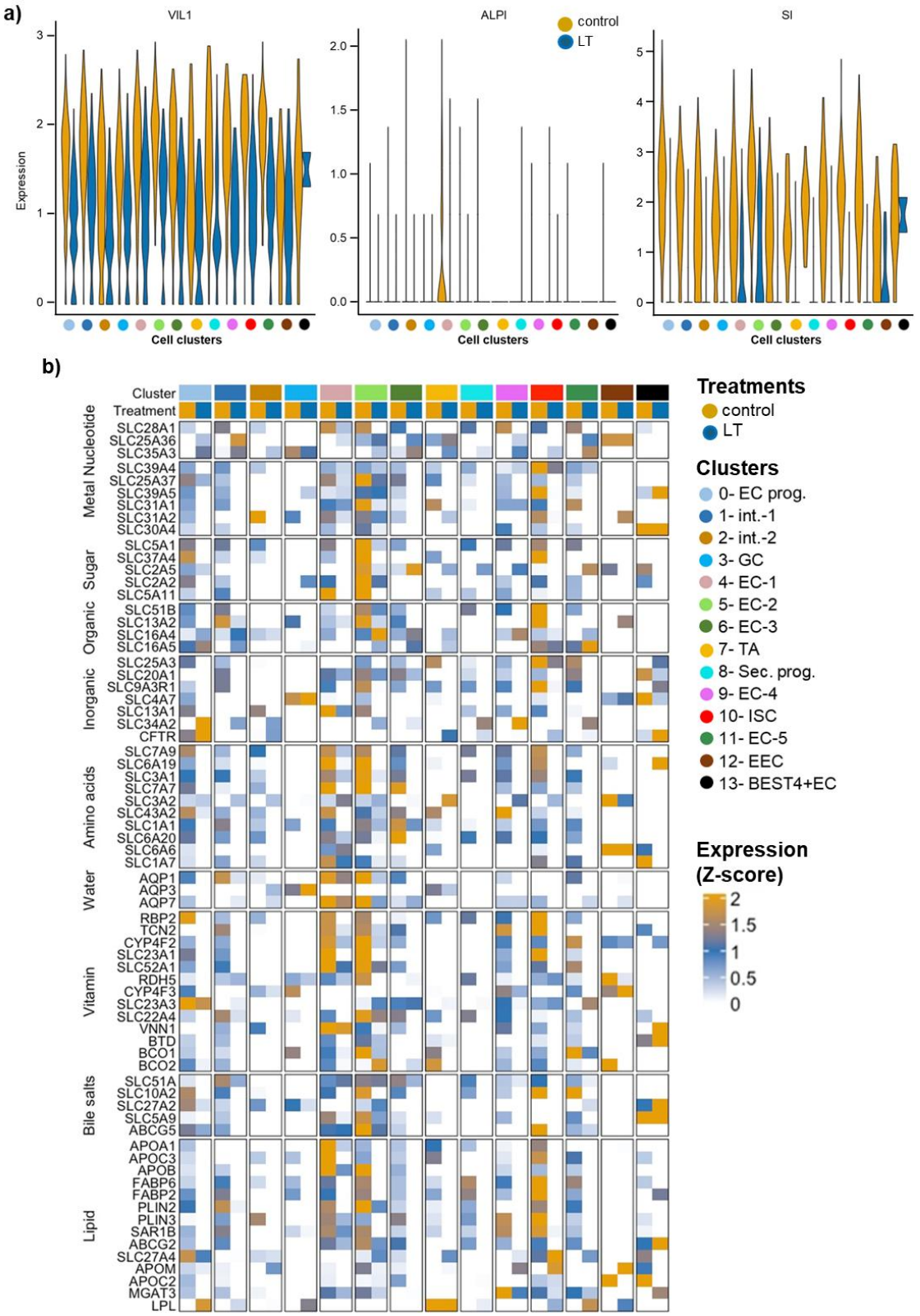

747

748 **Supplementary figure 6. LT impairs enterocyte maturation and suppresses expression of nutrient**

749 **transporters.**

750 **a)** Violin plots showing gene expression profile of mature enterocyte markers (VIL1, ALPI, and SI) in

751 control and LT-treated human ileal enteroids. Each panel displays normalized expression levels across the

752 epithelial cell clusters. **b)** Heatmap displaying expression profiles of nutrient transporter genes across all

753 clusters in control and LT-treated human ileal enteroids. Expression values represent Z-score of

754 SCTransform-normalized data averaged per cluster. Bars above the heatmap denote treatment (control,

755 LT) and cluster identities as indicated.

756

Supplementary figure 7

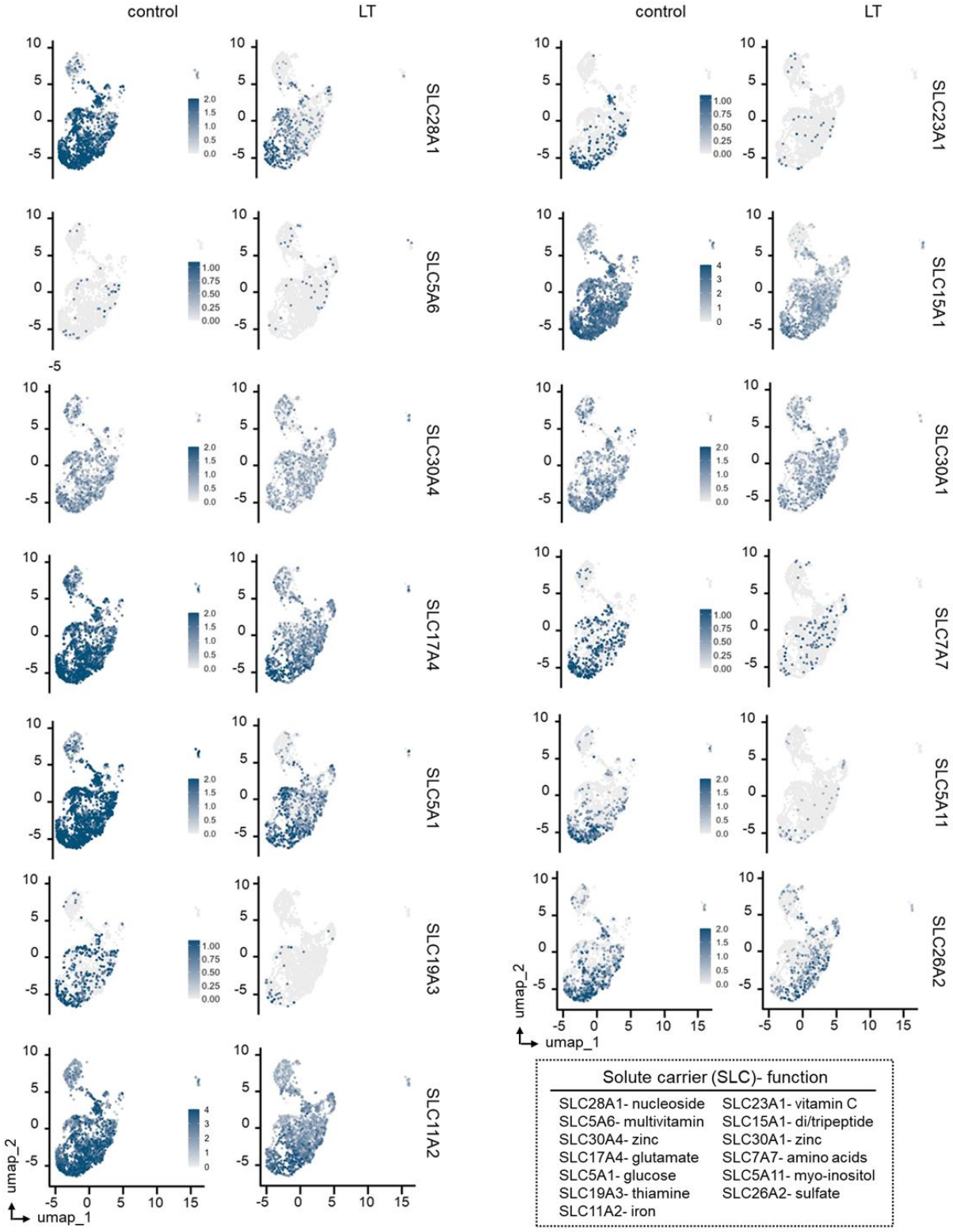

759 **Supplementary figure 7. LT suppresses expression of multiple nutrient transporter genes in human**

760 **ileal enteroids.**

761 UMAP feature plots showing the expression of select solute carrier (SLC) family genes involved in

762 nutrient absorption across control (left panels) and LT-treated (right panels) human ileal enteroids. Each

763 pair of panels displays normalized expression levels of a specific SLC gene projected onto the epithelial

764 cell landscape. Gene function annotations are summarized in the accompanying table.

765

766 ## Supplementary tables

767 **Supplementary table 1: Primer sequences used in Quantitative RT-PCR experiments**

Gene	PrimerBank ID*	direction	amplicon size	sequence	Source*
CTNNB1	148233337c2	F	150	CATCTACACAGTTTGATGCTGCT	PrimerBank
		R		GCAGTTTTGTCAGTTCAGGGA	PrimerBank
SOX9	182765453c1	F	85	AGCGAACGCACATCAAGAC	PrimerBank
		R		CTGTAGGCGATCTGTTGGGG	PrimerBank
OLFM4	325053703c2	F	135	ACTGTCCGAATTGACATCATGG	PrimerBank
		R		TTCTGAGCTTCCACCAAAACTC	PrimerBank
MYC	239582723c1	F	119	GGCTCCTGGCAAAAGGTCA	PrimerBank
		R		CTGCGTAGTTGTGCTGATGT	PrimerBank
CCND1	77628152c1	F	135	GCTGCGAAGTGGAAACCATC	PrimerBank
		R		CCTCCTTCTGCACACATTTGAA	PrimerBank
CD24	73623396c1	F	166	CTCCTACCCACGCAGATTTATTC	PrimerBank
		R		AGAGTGAGACCACGAAGAGAC	PrimerBank
PROM1	224994190c1	F	99	AGTCGGAAACTGGCAGATAGC	PrimerBank
		R		GGTAGTGTTGTACTGGGCCAAT	PrimerBank
CEACAM6	NA	F	113	CACCGTCGGCATCACGA	[29]
	NA	R		GAAGAATTCAGGGTCTGGTCCA	[29]
*https://pga.mgh.harvard.edu/primerbank/index.html					

768

769

770 **Supplementary table 2: Antibody descriptions and sources for immunoblot and fluorescence**

771 **microscopy experiments**

Protein, antigen	clone[1]	host	isotype	conjugation	source	RRID*
GAPDH, C terminal peptide	m |14C10	Rabbit	IgG		Cell Signaling 2118S	AB_561053
GSK-3a/b (synthetic peptide surrounding Gln269 of human GSK-3a protein)	D75D3	Rabbit	IgG		Cell Signaling 5676	AB_10547140
GSK-3b Ser_9 phospho-peptide	polyclonal	Rabbit	IgG		Cell Signaling 9336S	AB_331405
GSK-3a/b (Ser21/9) synthetic phophopeptides	Polyclonal	Rabbit			Cell Signaling 9331	AB_329830
b-catenin (synthetic peptide circa Pro174 of human protein)	monoclonal (D10A8)	Rabbit	IgG		Cell Signaling 8480	AB_11127855
b-catenin Ser_{675} C-terminal phospho-peptide	polyclonal	Rabbit	IgG		Invitrogen PA5-77933	AB_2736355
MKI67	polyclonal	Rabbit	IgG		Novus NB500-170	AB_10001977
Villin (BDID2C3)	monoclonal	Mouse	IgG1		Santa Cruz sc-66022	AB_2216247
ALPI	polyclonal	Rabbit	IgG		Invitrogen PA5-22210	AB_11153471
GAPDH (14C10)	monoclonal	Rabbit			Cell Signaling 2118S	AB_561053
Lamin B1	monoclonal (EPR22165-121)	Rabbit	IgG		Abcam ab229025	AB_3083735
Anti-rabbit IgG	polyclonal	Goat	IgG (H+L)	Alexa Fluor 488	ThermoFisher A-11070	AB_143165
Anti-rabbit IgG	polyclonal	Goat	IgG	HRP	Cell Signaling 7074S	AB_2099233
Anti-mouse IgG	polyclonal	Horse	IgG	HRP	Cell Signaling 7076S	AB_330924

772 * https://rrid.site/

773 **Supplementary table 3: Plasmids used in the construction of TCF/LEF reporter enteroid lines**

plasmid	description	source	reference
psPAX2	2nd generation lentiviral packaging plasmid	addgene[1]	
pMD2.G	VSV-G envelope expressing plasmid for lentiviral packaging	addgene[2]	
p7TFP	7X copies of the TCF/LEF transcriptional response element GATCAAAGG linked to firefly luciferase ; puromycin R	addgene[3]	[30]

[1]psPAX2 was a gift from Didier Trono (https://www.addgene.org/12260/; RRID:Addgene_12260)
[2]pMD2.G was a gift from Didier Trono (https://www.addgene.org/12259/ ; RRID:Addgene_12259)
[3]p7TFP was a gift from Roel Nusse (https://www.addgene.org/24308/; RRID:Addgene_24308)

774
775
776

Supplementary table 4: links to the original images and datasets

Type	Description	DOI
Figure 2b-c.	Original blots of β-catenin, phospho-β-catenin- Ser_{675}, GSK3β, phospho-GSK3β-Ser_9, Lamin-b1, and GAPDH	10.6084/m9.figshare.30100273
Figure 6a.	Original blot of intestinal alkaline phosphatase (ALPI)	10.6084/m9.figshare.30104512
Figure 6b.	Original blot of Villin	10.6084/m9.figshare.30104635
Data	Data associated with graphs	10.6084/m9.figshare.30198553
Data	Data associated with tables	10.6084/m9.figshare.30201280

Acknowledgements

JMF was supported by funding from the Department of Veterans Affairs (VA) (5I01BX001469-05), and the National Institute of Allergy and Infectious Diseases (NIAID) of the National Institutes of Health (NIH) R01 AI170949, R01 AI089894, and support by the NIH Washington University DDRCC Grant NIDDK P30 DK052574. AS was supported by National Institute of Allergy and Infectious Diseases of the National Institutes of Health under Award Number T32AI007172 and JIT1052 (supported by the Washington University Institute of Clinical and Translational Sciences grant UL1TR002345 from the National Center for Advancing Translational Sciences (NCATS) of the NIH. We thank the Genome Technology Access Center at the McDonnell Genome Institute at Washington University School of Medicine for help with genomic analysis. The Center is partially supported by NCI Cancer Center Support Grant #P30 CA91842 to the Siteman Cancer Center from the National Center for Research Resources (NCRR), a component of the NIH, and NIH Roadmap for Medical Research. This publication is solely the responsibility of the authors and does not necessarily represent the official view of NCRR, NIH, or VA.

References

1 Fleckenstein, J. M. & Sheikh, A. Emerging Themes in the Molecular Pathogenesis of Enterotoxigenic Escherichia coli. *J Infect Dis* (2021). https://doi.org/10.1093/infdis/jiab359

2 Khalil, I. A. *et al.* Morbidity and mortality due to shigella and enterotoxigenic Escherichia coli diarrhoea: the Global Burden of Disease Study 1990-2016. *Lancet Infect Dis* **18**, 1229-1240 (2018). https://doi.org/10.1016/S1473-3099(18)30475-4

3 Qadri, F. *et al.* Disease burden due to enterotoxigenic Escherichia coli in the first 2 years of life in an urban community in Bangladesh. *Infection and immunity* **75**, 3961-3968 (2007). https://doi.org/10.1128/IAI.00459-07

4 Kotloff, K. L. *et al.* Burden and aetiology of diarrhoeal disease in infants and young children in developing countries (the Global Enteric Multicenter Study, GEMS): a prospective, case-control study. *Lancet* **382**, 209-222 (2013). https://doi.org/10.1016/S0140-6736(13)60844-2

5 Levine, M. M. *et al.* Diarrhoeal disease and subsequent risk of death in infants and children residing in low-income and middle-income countries: analysis of the GEMS case-control study and 12-month GEMS-1A follow-on study. *Lancet Glob Health* **8**, e204-e214 (2020). https://doi.org/10.1016/S2214-109X(19)30541-8

6 Nasrin, D. *et al.* Pathogens associated with linear growth faltering in children with diarrhea and impact of antibiotic treatment: The Global Enteric Multicenter Study. *J Infect Dis* (2021). https://doi.org/10.1093/infdis/jiab434

7 Kotloff, K. L. *et al.* The incidence, aetiology, and adverse clinical consequences of less severe diarrhoeal episodes among infants and children residing in low-income and middle-income countries: a 12-month case-control study as a follow-on to the Global Enteric Multicenter Study (GEMS). *Lancet Glob Health* **7**, e568-e584 (2019). https://doi.org/10.1016/S2214-109X(19)30076-2

8 Amadi, B. *et al.* Adaptation of the small intestine to microbial enteropathogens in Zambian children with stunting. *Nat Microbiol* **6**, 445-454 (2021). https://doi.org/10.1038/s41564-020-00849-w

9 Kelly, P. *et al.* Histopathology underlying environmental enteric dysfunction in a cohort study of undernourished children in Bangladesh, Pakistan, and Zambia compared with United States children. *Am J Clin Nutr* **120 Suppl 1**, S15-S30 (2024). https://doi.org/10.1016/j.ajcnut.2024.02.028

10 Sheikh, A. *et al.* Enterotoxigenic Escherichia coli heat-labile toxin drives enteropathic changes in small intestinal epithelia. *Nature communications* **13**, 6886 (2022). https://doi.org/https://doi.org/10.1038/s41467-022-34687-7

11 Haber, A. L. *et al.* A single-cell survey of the small intestinal epithelium. *Nature* **551**, 333-339 (2017). https://doi.org/10.1038/nature24489

12 Mariadason, J. M. *et al.* Gene expression profiling of intestinal epithelial cell maturation along the crypt-villus axis. *Gastroenterology* **128**, 1081-1088 (2005). https://doi.org/10.1053/j.gastro.2005.01.054

13 Moor, A. E. *et al.* Spatial Reconstruction of Single Enterocytes Uncovers Broad Zonation along the Intestinal Villus Axis. *Cell* **175**, 1156-1167 e1115 (2018). https://doi.org/10.1016/j.cell.2018.08.063

14 Yu, J. *et al.* Environmental Enteric Dysfunction Includes a Broad Spectrum of Inflammatory Responses and Epithelial Repair Processes. *Cell Mol Gastroenterol Hepatol* **2**, 158-174 e151 (2016). https://doi.org/10.1016/j.jcmgh.2015.12.002

15 George, C. M. *et al.* Enteric Infections in Young Children are Associated with Environmental Enteropathy and Impaired Growth. *Trop Med Int Health* **23**, 26-33 (2018). https://doi.org/10.1111/tmi.13002

16 Guerrant, R. L., Oria, R. B., Moore, S. R., Oria, M. O. & Lima, A. A. Malnutrition as an enteric infectious disease with long-term effects on child development. *Nutr Rev* **66**, 487-505 (2008). https://doi.org/10.1111/j.1753-4887.2008.00082.x

17 Rosenberg, I. H., Solomons, N. W. & Schneider, R. E. Malabsorption associated with diarrhea and intestinal infections. *Am J Clin Nutr* **30**, 1248-1253 (1977). https://doi.org/10.1093/ajcn/30.8.1248

18 van der Flier, L. G. & Clevers, H. Stem cells, self-renewal, and differentiation in the intestinal epithelium. *Annu Rev Physiol* **71**, 241-260 (2009). https://doi.org/10.1146/annurev.physiol.010908.163145

19 Fevr, T., Robine, S., Louvard, D. & Huelsken, J. Wnt/beta-catenin is essential for intestinal homeostasis and maintenance of intestinal stem cells. *Molecular and cellular biology* **27**, 7551-7559 (2007). https://doi.org/10.1128/MCB.01034-07

20 Van der Flier, L. G. *et al.* The Intestinal Wnt/TCF Signature. *Gastroenterology* **132**, 628-632 (2007). https://doi.org/10.1053/j.gastro.2006.08.039

21 Vanuytsel, T., Senger, S., Fasano, A. & Shea-Donohue, T. Major signaling pathways in intestinal stem cells. *Biochim Biophys Acta* **1830**, 2410-2426 (2013). https://doi.org/10.1016/j.bbagen.2012.08.006

22 Farin, H. F. *et al.* Visualization of a short-range Wnt gradient in the intestinal stem-cell niche. *Nature* **530**, 340-343 (2016). https://doi.org/10.1038/nature16937

23 Winston, J. T. *et al.* The SCFbeta-TRCP-ubiquitin ligase complex associates specifically with phosphorylated destruction motifs in IkappaBalpha and beta-catenin and stimulates IkappaBalpha ubiquitination in vitro. *Genes Dev* **13**, 270-283 (1999). https://doi.org/10.1101/gad.13.3.270

24 Taipale, J. & Beachy, P. A. The Hedgehog and Wnt signalling pathways in cancer. *Nature* **411**, 349-354 (2001). https://doi.org/10.1038/35077219

25 Papkoff, J., Rubinfeld, B., Schryver, B. & Polakis, P. Wnt-1 regulates free pools of catenins and stabilizes APC-catenin complexes. *Molecular and cellular biology* **16**, 2128-2134 (1996). https://doi.org/10.1128/MCB.16.5.2128

26 Korinek, V. *et al.* Constitutive transcriptional activation by a beta-catenin-Tcf complex in APC-/- colon carcinoma. *Science* **275**, 1784-1787 (1997). https://doi.org/10.1126/science.275.5307.1784

27 Wang, Y. *et al.* Single-cell transcriptome analysis reveals differential nutrient absorption functions in human intestine. *J Exp Med* **217** (2020). https://doi.org/10.1084/jem.20191130

28 Beumer, J. & Clevers, H. Cell fate specification and differentiation in the adult mammalian intestine. *Nat Rev Mol Cell Biol* **22**, 39-53 (2021). https://doi.org/10.1038/s41580-020-0278-0

29 Sheikh, A. *et al.* CEACAMs serve as toxin-stimulated receptors for enterotoxigenic Escherichia coli. *Proc Natl Acad Sci U S A* **117**, 29055-29062 (2020). https://doi.org/10.1073/pnas.2012480117

30 Fuerer, C. & Nusse, R. Lentiviral vectors to probe and manipulate the Wnt signaling pathway. *PLoS One* **5**, e9370 (2010). https://doi.org/10.1371/journal.pone.0009370

31 Cadigan, K. M. & Waterman, M. L. TCF/LEFs and Wnt signaling in the nucleus. *Cold Spring Harb Perspect Biol* **4** (2012). https://doi.org/10.1101/cshperspect.a007906

32 Hino, S., Tanji, C., Nakayama, K. I. & Kikuchi, A. Phosphorylation of beta-catenin by cyclic AMP-dependent protein kinase stabilizes beta-catenin through inhibition of its ubiquitination. *Molecular and cellular biology* **25**, 9063-9072 (2005). https://doi.org/10.1128/MCB.25.20.9063-9072.2005

33 Li, M. *et al.* Cyclic AMP promotes neuronal survival by phosphorylation of glycogen synthase kinase 3beta. *Molecular and cellular biology* **20**, 9356-9363 (2000). https://doi.org/10.1128/MCB.20.24.9356-9363.2000

34 Fang, X. *et al.* Phosphorylation and inactivation of glycogen synthase kinase 3 by protein kinase A. *Proc Natl Acad Sci U S A* **97**, 11960-11965 (2000). https://doi.org/10.1073/pnas.220413597

35 Tanji, C. *et al.* A-kinase anchoring protein AKAP220 binds to glycogen synthase kinase-3beta (GSK-3beta) and mediates protein kinase A-dependent inhibition of GSK-3beta. *The Journal of biological chemistry* **277**, 36955-36961 (2002). https://doi.org/10.1074/jbc.M206210200

36 Suzuki, A. *et al.* PTH/cAMP/PKA signaling facilitates canonical Wnt signaling via inactivation of glycogen synthase kinase-3beta in osteoblastic Saos-2 cells. *J Cell Biochem* **104**, 304-317 (2008). https://doi.org/10.1002/jcb.21626

37 Wang, S. *et al.* Quantitative Phosphoproteomic Study Reveals that Protein Kinase A Regulates Neural Stem Cell Differentiation Through Phosphorylation of Catenin Beta-1 and Glycogen Synthase Kinase 3beta. *Stem Cells* **34**, 2090-2101 (2016). https://doi.org/10.1002/stem.2387

38 Kawasaki, Y. *et al.* Phosphorylation of GSK-3beta by cGMP-dependent protein kinase II promotes hypertrophic differentiation of murine chondrocytes. *The Journal of clinical investigation* **118**, 2506-2515 (2008). https://doi.org/10.1172/JCI35243

39 Zhao, X., Zhuang, S., Chen, Y., Boss, G. R. & Pilz, R. B. Cyclic GMP-dependent protein kinase regulates CCAAT enhancer-binding protein beta functions through inhibition of glycogen synthase kinase-3. *The Journal of biological chemistry* **280**, 32683-32692 (2005). https://doi.org/10.1074/jbc.M505486200

40 Taurin, S., Sandbo, N., Yau, D. M., Sethakorn, N. & Dulin, N. O. Phosphorylation of beta-catenin by PKA promotes ATP-induced proliferation of vascular smooth muscle cells. *Am J Physiol Cell Physiol* **294**, C1169-1174 (2008). https://doi.org/10.1152/ajpcell.00096.2008

41 Taurin, S., Sandbo, N., Qin, Y., Browning, D. & Dulin, N. O. Phosphorylation of beta-catenin by cyclic AMP-dependent protein kinase. *The Journal of biological chemistry* **281**, 9971-9976 (2006). https://doi.org/10.1074/jbc.M508778200

42 Zambon, A. C. *et al.* Gene expression patterns define key transcriptional events in cell-cycle regulation by cAMP and protein kinase A. *Proc Natl Acad Sci U S A* **102**, 8561-8566 (2005). https://doi.org/10.1073/pnas.0503363102

43 Hua, X. *et al.* A Ctnnb1 enhancer transcriptionally regulates Wnt signaling dosage to balance homeostasis and tumorigenesis of intestinal epithelia. *Elife* **13** (2024). https://doi.org/10.7554/eLife.98238

44 Sanman, L. E. *et al.* Transit-Amplifying Cells Coordinate Changes in Intestinal Epithelial Cell-Type Composition. *Dev Cell* **56**, 356-365 e359 (2021). https://doi.org/10.1016/j.devcel.2020.12.020

45 Satija, R., Farrell, J. A., Gennert, D., Schier, A. F. & Regev, A. Spatial reconstruction of single-cell gene expression data. *Nat Biotechnol* **33**, 495-502 (2015). https://doi.org/10.1038/nbt.3192

46 Butler, A., Hoffman, P., Smibert, P., Papalexi, E. & Satija, R. Integrating single-cell transcriptomic data across different conditions, technologies, and species. *Nat Biotechnol* **36**, 411-420 (2018). https://doi.org/10.1038/nbt.4096

47 Scholzen, T. & Gerdes, J. The Ki-67 protein: from the known and the unknown. *J Cell Physiol* **182**, 311-322 (2000). https://doi.org/10.1002/(SICI)1097-4652(200003)182:3<311::AID-JCP1>3.0.CO;2-9

48 Olsen, L., Bressendorff, S., Troelsen, J. T. & Olsen, J. Differentiation-dependent activation of the human intestinal alkaline phosphatase promoter by HNF-4 in intestinal cells. *American journal of physiology. Gastrointestinal and liver physiology* **289**, G220-226 (2005). https://doi.org/10.1152/ajpgi.00449.2004

49 Sheikh, A. *et al.* Enterotoxigenic Escherichia coli heat-labile toxin drives enteropathic changes in small intestinal epithelia. *Nature communications* **13**, 6886 (2022). https://doi.org/10.1038/s41467-022-34687-7

50 Platts-Mills, J. A. *et al.* Association between enteropathogens and malnutrition in children aged 6-23 mo in Bangladesh: a case-control study. *Am J Clin Nutr* **105**, 1132-1138 (2017). https://doi.org/10.3945/ajcn.116.138800

51 Rogawski, E. T. *et al.* Use of quantitative molecular diagnostic methods to investigate the effect of enteropathogen infections on linear growth in children in low-resource settings: longitudinal analysis of results from the MAL-ED cohort study. *Lancet Glob Health* **6**, e1319-e1328 (2018). https://doi.org/10.1016/S2214-109X(18)30351-6

52 Sheikh, A. *et al.* Enterotoxigenic Escherichia coli heat-labile toxin drives enteropathic changes in small intestinal epithelia. *Nature communications* **13**, 6886 (2022). https://doi.org/10.1038/s41467-022-34687-7

53 Valenta, T., Hausmann, G. & Basler, K. The many faces and functions of beta-catenin. *EMBO J* **31**, 2714-2736 (2012). https://doi.org/10.1038/emboj.2012.150

54 MacDonald, B. T., Tamai, K. & He, X. Wnt/beta-catenin signaling: components, mechanisms, and diseases. *Dev Cell* **17**, 9-26 (2009). https://doi.org/10.1016/j.devcel.2009.06.016

55 Fleckenstein, J. M. & Kuhlmann, F. M. Enterotoxigenic Escherichia coli Infections. *Curr Infect Dis Rep* **21**, 9 (2019). https://doi.org/10.1007/s11908-019-0665-x

56 Fleckenstein, J. M. *et al.* Molecular mechanisms of enterotoxigenic Escherichia coli infection. *Microbes Infect* **12**, 89-98 (2010). https://doi.org/S1286-4579(09)00235-4 [pii] 10.1016/j.micinf.2009.10.002

57 Chen, Y. *et al.* Ser9 phosphorylation of GSK-3beta promotes aging in the heart through suppression of autophagy. *J Cardiovasc Aging* **1** (2021). https://doi.org/10.20517/jca.2021.13

58 Fang, D. *et al.* Phosphorylation of beta-catenin by AKT promotes beta-catenin transcriptional activity. *J Biol Chem* **282**, 11221-11229 (2007). https://doi.org/10.1074/jbc.M611871200

59 Sassone-Corsi, P. The cyclic AMP pathway. *Cold Spring Harb Perspect Biol* **4** (2012). https://doi.org/10.1101/cshperspect.a011148

60 Brown, A. C. *et al.* The cAMP responsive element modulator (CREM) transcription factor influences susceptibility to undernutrition and infection. *mBio*, e0139025 (2025). https://doi.org/10.1128/mbio.01390-25

61 Vemuri, K., Radi, S. H., Sladek, F. M. & Verzi, M. P. Multiple roles and regulatory mechanisms of the transcription factor HNF4 in the intestine. *Front Endocrinol (Lausanne)* **14**, 1232569 (2023). https://doi.org/10.3389/fendo.2023.1232569

62 Sands, W. A. & Palmer, T. M. Regulating gene transcription in response to cyclic AMP elevation. *Cell Signal* **20**, 460-466 (2008). https://doi.org/10.1016/j.cellsig.2007.10.005

63 Alaullah Sheikh, B. T., Tim J Vickers, John C Martin, Bruce A Rosa, Subrata Sabui, Supratim Basu, Rita D Simoes, Makedonka Mitreva, Chad Storer, Erik Tyksen, Richard D Head, Wandy Beatty, Hamid M Said, James M Fleckenstein. Enterotoxigenic Escherichia coli heat-labile toxin drives enteropathic changes in small intestinal epithelia. *Nature communications* **Nov 12;13(1):6886** (2022). https://doi.org/https://doi.org/10.1038/s41467-022-34687-7

64 Chen, L. *et al.* A reinforcing HNF4-SMAD4 feed-forward module stabilizes enterocyte identity. *Nat Genet* **51**, 777-785 (2019). https://doi.org/10.1038/s41588-019-0384-0

65 Chen, L. *et al.* HNF4 factors control chromatin accessibility and are redundantly required for maturation of the fetal intestine. *Development* **146** (2019). https://doi.org/10.1242/dev.179432

66 Sansom, O. J. *et al.* Loss of Apc in vivo immediately perturbs Wnt signaling, differentiation, and migration. *Genes Dev* **18**, 1385-1390 (2004). https://doi.org/10.1101/gad.287404

67 Andreu, P. *et al.* Crypt-restricted proliferation and commitment to the Paneth cell lineage following Apc loss in the mouse intestine. *Development* **132**, 1443-1451 (2005). https://doi.org/10.1242/dev.01700

68 Malonga, T., Vialaneix, N. & Beaumont, M. BEST4(+) cells in the intestinal epithelium. *Am J Physiol Cell Physiol* **326**, C1345-C1352 (2024). https://doi.org/10.1152/ajpcell.00042.2024

69 Kelly, P. *et al.* Gene expression profiles compared in environmental and malnutrition enteropathy in Zambian children and adults. *EBioMedicine* **70**, 103509 (2021). https://doi.org/10.1016/j.ebiom.2021.103509

70 Mulenga, C. *et al.* Epithelial Abnormalities in the Small Intestine of Zambian Children With Stunting. *Front Med (Lausanne)* **9**, 849677 (2022). https://doi.org/10.3389/fmed.2022.849677

71 Zhao, X. *et al.* Bile Acid Profiling Reveals Distinct Signatures in Undernourished Children with Environmental Enteric Dysfunction. *J Nutr* **151**, 3689-3700 (2021). https://doi.org/10.1093/jn/nxab321

72 Malique, A. *et al.* NAD(+) precursors and bile acid sequestration treat preclinical refractory environmental enteric dysfunction. *Science translational medicine* **16**, eabq4145 (2024). https://doi.org/10.1126/scitranslmed.abq4145

73 Guerrant, R. L., Schorling, J. B., McAuliffe, J. F. & de Souza, M. A. Diarrhea as a cause and an effect of malnutrition: diarrhea prevents catch-up growth and malnutrition increases diarrhea frequency and duration. *Am J Trop Med Hyg* **47**, 28-35 (1992). https://doi.org/10.4269/ajtmh.1992.47.28

74 Owino, V. *et al.* Environmental Enteric Dysfunction and Growth Failure/Stunting in Global Child Health. *Pediatrics* **138** (2016). https://doi.org/10.1542/peds.2016-0641

75 Vonaesch, P. *et al.* Identifying the etiology and pathophysiology underlying stunting and environmental enteropathy: study protocol of the AFRIBIOTA project. *BMC Pediatr* **18**, 236 (2018). https://doi.org/10.1186/s12887-018-1189-5

1002 76 Rogawski, E. T. & Guerrant, R. L. The Burden of Enteropathy and "Subclinical" Infections. *Pediatr*
1003 *Clin North Am* **64**, 815-836 (2017). https://doi.org/10.1016/j.pcl.2017.03.003
1004 77 Kosek, M. N. & Investigators, M.-E. N. Causal Pathways from Enteropathogens to Environmental
1005 Enteropathy: Findings from the MAL-ED Birth Cohort Study. *EBioMedicine* **18**, 109-117 (2017).
1006 https://doi.org/10.1016/j.ebiom.2017.02.024
1007 78 Black, R. E., Brown, K. H. & Becker, S. Effects of diarrhea associated with specific enteropathogens
1008 on the growth of children in rural Bangladesh. *Pediatrics* **73**, 799-805 (1984).
1009 79 Li, P. *et al.* Homeostatic control of the crypt-villus axis by the bacterial enterotoxin receptor
1010 guanylyl cyclase C restricts the proliferating compartment in intestine. *The American journal of*
1011 *pathology* **171**, 1847-1858 (2007). https://doi.org/10.2353/ajpath.2007.070198
1012 80 Pitari, G. M. *et al.* Bacterial enterotoxins are associated with resistance to colon cancer. *Proc Natl*
1013 *Acad Sci U S A* **100**, 2695-2699 (2003). https://doi.org/10.1073/pnas.0434905100
1014 81 Pitari, G. M., Di Guglielmo, M. D., Park, J., Schulz, S. & Waldman, S. A. Guanylyl cyclase C agonists
1015 regulate progression through the cell cycle of human colon carcinoma cells. *Proc Natl Acad Sci U*
1016 *S A* **98**, 7846-7851 (2001). https://doi.org/10.1073/pnas.141124698
1017 82 Pasetti, M. F. *et al.* Safety and immunogenicity in humans of enterotoxigenic Escherichia coli
1018 double mutant heat-labile toxin administered intradermally. *NPJ Vaccines* **10**, 23 (2025).
1019 https://doi.org/10.1038/s41541-025-01071-7
1020 83 VanDussen, K. L. *et al.* Development of an enhanced human gastrointestinal epithelial culture
1021 system to facilitate patient-based assays. *Gut* **64**, 911-920 (2015). https://doi.org/10.1136/gutjnl-
1022 2013-306651
1023 84 Miyoshi, H. & Stappenbeck, T. S. In vitro expansion and genetic modification of gastrointestinal
1024 stem cells in spheroid culture. *Nat Protoc* **8**, 2471-2482 (2013).
1025 https://doi.org/10.1038/nprot.2013.153
1026 85 McGinnis, C. S., Murrow, L. M. & Gartner, Z. J. DoubletFinder: Doublet Detection in Single-Cell RNA
1027 Sequencing Data Using Artificial Nearest Neighbors. *Cell Syst* **8**, 329-337 e324 (2019).
1028 https://doi.org/10.1016/j.cels.2019.03.003
1029 86 Hafemeister, C. & Satija, R. Normalization and variance stabilization of single-cell RNA-seq data
1030 using regularized negative binomial regression. *Genome Biol* **20**, 296 (2019).
1031 https://doi.org/10.1186/s13059-019-1874-1
1032 87 Tirosh, I. *et al.* Dissecting the multicellular ecosystem of metastatic melanoma by single-cell RNA-
1033 seq. *Science* **352**, 189-196 (2016). https://doi.org/10.1126/science.aad0501
1034